Studies of Large Scale Atmospheric Energetics

Department of Meteorology
University of Wisconsin–Madison
1225 West Dayton Street
Madison, Wisconsin 53706

Contributions by

E. G. Astling
L. H. Horn
T. A. MacKenzie
W. E. Togstad

L. H. Horn and D. R. Johnson, Joint Principal Investigators

FINAL REPORT

The research in this document has been supported by the National Environmental Satellite Service of the National Oceanic and Atmospheric Administration under Grant 1-35229

August 1972

Studies of Large Scale

Atmospheric Energetics

Department of Meteorology
The University of Wisconsin—Madison
1225 W. Dayton Street
Madison, Wisconsin 53706

Contributions by

E. G. Astling
L. H. Horn
T. A. MacKenzie
W. E. Togstad

L. H. Horn and D. R. Johnson, Joint Principal Investigators

Final Report

The research in this document has been supported
by the National Environmental Satellite Service of the
National Oceanic and Atmospheric Administration under Grant 1-35229

August 1972

Scanner's note:

This page is blank.

Table of Contents

Scanner's note:

This page is blank.

Introduction

The research presented in this report consists of the final studies conducted with the support of NOAA Grant 1-35229. Some of the work reported here was initiated with support from ESSA Grant E-8-69(G) which immediately preceded this NOAA grant. The research represents the continuing effort to describe the energetics of the large-scale motions of the atmosphere with particular emphasis given to the employment of meteorological satellite data to the problem.

Because of the delay in the publication of this final report, the paper "Atmospheric Energy Transport over North America for Three Winter Months, " by Astling and Horn has already been published. It is reprinted here with the permission of the Editor of the Monthly Weather Review. The study concentrates on the various modes of the poleward energy transport in the North American region and on the importance of various large-scale synoptic features to the transport.

An important part of this project's research effort over the past decade has been the investigation of the generation of available potential energy by the various diabatic processes. In one of the earliest studies, Tiros II data and the approximate form of the generation equation were used to estimate the generation due to infrared cooling (Corcoran and Horn, 1965; Johnson, 1967). In later studies, the exact form of the generation equation was used to examine the importance of latent and sensible heating in the generation of available potential energy (Bullock and Johnson, 1971; Gall and Johnson, 1971; Anthes and Johnson, 1968; Dutton and Johnson, 1967). In this final report the article by MacKenzie and Horn again returns to the problem of examining the role of infrared cooling in generating available potential energy at the storm scale. However, in this study the exact form of the generation equation and Nimbus II infrared observations are employed.

The study by Togstad and Horn demonstrates the ability of the indirect sounding technique to describe the thermal support of the propagating jet streak, an important weather-producing circulation feature of the

atmosphere. To a degree, this study represents an application of the indirect sounding procedure which was developed by Smith (1967).

The work by Smith (1967) mentioned above in developing a procedure for inferring the thermal structure of the troposphere from satellite-measured irradiances represents one of the major contributions in the field of meteorology in recent years. This study was not only supported by the project, but also evolved from his earlier study relating satellite infrared reduction measurements to the infrared cooling in various layers of the atmosphere which was also done as part of the project. See Smith, Horn and Johnson (1966).

The work included in this report has received indirect support from the Wisconsin Alumni Research Foundation and the National Science Foundation in the form of grants to the University of Wisconsin's computing facility.

References

Anthes, R. A. and D. R. Johnson, 1968: Generation of available potential energy in hurricane Hilda (1964), MWR, Vol. 96, No. 5, pp. 291-305.

Bullock, B. R. and D. R. Johnson, 1971: The generation of available potential energy by latent heat release in a mid-latitude cyclone, MWR, Vol. 99, No. 1.

Corcoran, J. L. and L. H. Horn, 1965: The role of synoptic scale variations of infrared radiation in the generation of available potential energy, J. Geoph. Res., Vol. 70, No. 18.

Dutton, J. A. and D. R. Johnson, 1967: The theory of available potential energy and a variational approach to atmospheric energetics, Adv. in Geoph., Vol. 12.

Gall, R. L. and D. R. Johnson, 1971: The generation of available potential energy by sensible heating: A case study, Tellus, Vol. 23, pp. 466-482.

Johnson, D. R., 1967: The role of terrestrial radiation in the generation of zonal and eddy available potential energy, Tellus, Vol. 19, No. 4, pp. 517-539.

Smith, W. L., L. H. Horn, and D. R. Johnson, 1966: On the relation between Tiros radiative measurements and atmospheric infrared cooling, J. App. Met., Vol. 5, No. 4.

Smith, W. L., 1967: An iterative method for deducing tropospheric temperature and moisture profiles from satellite radiation measurements, MWR, Vol. 5, No. 6, pp. 363-369.

General Acknowledgments

The series of grants from the U. S. Weather Bureau, ESSA and NOAA which have supported this project date back to 1961. During this time the project has made significant contributions to an understanding of the atmosphere's energy processes and to the employment of meteorological satellites. In turn, numerous individual members of the project have benefited from the support. Perhaps the most important aspect of this fruitful relationship has been the support provided for a number of University of Wisconsin graduate students. Today most of these former students are engaged in meteorological research, teaching or operations in a variety of positions. As students, the following received project support in the form of research assistantships:

E. G. Astling, M. S., Ph. D
B. R. Bullock, M. S., Ph. D
A. Carasso, M. S.
R. L. Gall, M. S.
G. Gutman, M. S.
D. G. Hahn, M. S.
D. R. Johnson, Ph. D.
R. C. Lo, M. S., Ph. D.
T. A. MacKenzie, M. S.
P. J. Schmidt, M. S.
P. J. Smith, M. S., Ph. D.
W. L. Smith, M. S., Ph. D.
W. E. Togstad, M. S.

Some form of project support was also provided for the masters degree research of J. L. Corcoran, G. J. Dittberner, R. A. Rudy and R. A. Anthes and the Ph. D. work of J. A. Dutton. In addition to the work of the Joint Principal Investigators (Horn and Johnson), the series of grants have at one time or another briefly supported some aspects of the research of R. J. Deland, W. S. Schwerdtfeger, W. C. Shen, and F. Sechrist.

This long period of support by the National Environmental Satellite Service is gratefully acknowledged.

Lyle H. Horn
Donald R. Johnson
Joint Principal Investigators

Madison, Wisconsin
August 1972

Reprinted from MONTHLY WEATHER REVIEW, Vol. 100, No. 6, June 1972, pp. 491-502.

Atmospheric Energy Transport Over North America For Three Winter Months

ELFORD G. ASTLING—*Department of Meteorology, Florida State University, Tallahassee, Fla.*

LYLE H. HORN—*Department of Meteorology, University of Wisconsin, Madison, Wis.*

ABSTRACT—The excellent North American radiosonde network is used to calculate the poleward energy transport for the continental area during the period January–March 1966. The transport of sensible and latent heat and geopotential and kinetic energy is partitioned according to four circulation modes—mean and transient meridional circulations and stationary and transient eddy circulations. In addition, the roles of various synoptic features in the transient eddy flux are examined.

The mean meridional transport was computed in two ways. One involved a calculation of the contribution of the North American sector to the hemispheric mean meridional transport. Because of strong meridional flow at high levels and a lack of compensating flow at low levels, very large transports were obtained. The transports were much greater than the average for the entire hemisphere and point up the helical structure of the meridional cells. To obtain comparisons with other modes of transport, we made another calculation of the mean meridional transport by subtracting the vertical mean component from the longitudinal average. The results show that the energy transports were large and positive in subtropical latitudes and were zero or small and negative in middle latitudes.

Of the remaining modes, the transient eddy mode was the most effective in transporting energy poleward. The maximum transport occurred at 40°N for both the hemisphere and for North America; however, the value for North America was about 50 percent larger and the latitudinal variation was considerably greater than for the hemisphere. Sensible heat transport was largest, with the maximum latent transport amounting to one-half the sensible heat. Energy fluxes by the standing eddy and transient meridional modes were relatively small.

A brief study of the importance of various large-scale synoptic features in transporting energy indicated that large-amplitude troughs with closed 500-mb Lows are most effective in the transient eddy transport. Indications exist that the largest poleward energy transport is accomplished during the intensifying stage of baroclinic disturbances associated with the 500-mb Lows.

1. INTRODUCTION

One of the more prominent features of the atmospheric energy budget is the radiative energy surplus in low latitudes and deficit in high latitudes. Nearly all of the low-latitude surplus is converted into sensible heat, latent heat, and geopotential energy and is transported poleward by various transfer mechanisms in the atmosphere and oceans. In this paper, the characteristics of the energy transport for the North American sector of the Northern Hemisphere are studied for a 3-mo winter period.

Early theories of the general circulation of the atmosphere suggested that the mean meridional circulation was the principal mechanism in the poleward flux of energy. The work of a number of investigators, particularly those associated with the General Circulation Project at the Massachusetts Institute of Technology, has led to the currently accepted view that in middle and high latitudes the poleward transport is accomplished primarily by large-scale eddies. However, it is generally agreed that, equatorward of latitude 30°, the mean meridional cell is the basic transport mechanism, being especially pronounced in the winter season. For discussions of the various mechanisms of the poleward flux of energy, see, for example, Starr and White (1954), Peixoto (1960), Smagorinsky (1964), Holopainen (1965), and Oort (1971*a*).

Since most investigations dealing with energy transports involve estimates based on analyses extending over the entire Northern Hemisphere, certain uncertainties exist due to the sparse observation network over oceanic regions. In the Northern Hemisphere, for example, nearly half of the middle latitudes is covered by oceans, with few radiosonde and rawin stations. Holopainen (1968) found that, over data-sparse oceanic regions in the Northern Hemisphere, large differences exist between atmospheric flow statistics obtained from conventional and objective analyses.

In this paper, the poleward energy transport within the layer between the surface and 100 mb is studied for the months of January, February, and March 1966 for the major portion of the North American continent. By confining the study to this area of the Northern Hemisphere, statistics are obtained that are based on the best observational network available. Since the area covers only a sector of the Northern Hemisphere, the study is limited in that the statistics obtained represent only a contribution to the hemispheric energy transport. However, the values obtained are useful in making comparisons with statistics obtained from studies based on a lower quality hemisphere-wide data network. Such comparisons reveal the significant variations that exist in the modes of the energy transport in different longitudinal sectors.

Specifically, this study examines the transport of each of four energy forms by each of four modes of circulation. In addition, the energy fluxes associated with several types of large-amplitude, upper level wave patterns are briefly examined for some individual synoptic cases.

2. MATHEMATICAL FORMULATION OF THE TRANSPORT

Within the atmosphere, energy is transported as sensible heat, latent heat, geopotential energy, and kinetic energy. The total horizontal energy transport (Π_t) across a given latitude circle between the surface (p_0) and 100-mb levels can be written as

$$\Pi_t=\frac{1}{g}\oint\int_{p_0}^{100\text{ mb}}\left(c_pT+\Phi+Lq+\frac{\mathbf{V}\cdot\mathbf{V}}{2}\right)v\,dp\,dx \qquad (1)$$

where T denotes temperature, c_p is specific heat at constant pressure, Φ is geopotential energy per unit mass, q is specific humidity, L is latent heat, $\mathbf{V}$ is the horizontal wind vector, v is the meridional wind component, and x is the distance along a latitude circle.

The sensible heat term is typically the largest of the four energy forms at all levels between 1000 and 100 mb; however, at 100 mb, the geopotential energy term approaches the magnitude of the sensible heat. Near the lower boundary, the latent heat term may be as large as one-tenth of the total energy. Although the kinetic energy is small, its contribution to the poleward transport may be as large as geopotential energy fluxes at high levels for some circulation modes. For estimates of the atmospheric energy content as a function of height and latitude, see Oort (1971*a*).

If we let E_t represent one form of energy per unit mass, then the total energy content per unit mass is

$$E=\sum_{i=1}^{4}E_t \qquad (2)$$

where $i=1,\ldots,4$ denotes the four energy forms presented in eq (1).

To partition the poleward transport of energy according to circulation modes, we follow Lorenz (1967). Thus, for example, one of the energy forms may be expressed as

$$E_t=\{\overline{E}_t\}+\overline{E}_t^*+\{E_t\}'+\overline{E_t'^*} \qquad (3)$$

where $\{\}$ is an average with respect to longitude, $(^*)$ is a departure from a longitudinal average, $\bar{(\ )}$ is a time average, and $(')$ is a deviation from a time average.

Using eq (1) and (3), the poleward flux of a given energy form, Π_t, averaged with respect to longitude and time is

$$\{\overline{\Pi}_t\}=\frac{1}{g}\int_{p_0}^{100\text{ mb}}(\{\overline{E}_t\}\{\bar{v}\}+\{\overline{E}_t^*\bar{v}^*\}+\overline{\{E_t\}'\{v\}'}+\overline{\{E_t'^*v'^*\}})\,dp. \qquad (4)$$

The total energy transport is obtained by replacing E_t by E. The first term on the right side of eq (4) represents the poleward flux by the mean meridional motion over the limited region of study. The second term gives the transport by the standing or stationary eddies (e.g., semipermanent subtropical high-pressure systems and certain planetary waves of middle latitudes). The third term represents the transport by the transient meridional circulation; for example, the expansion and contraction of the circumpolar vortex with respect to time over the limited region of study. The last term represents the transport associated with transient eddies that appear as moving cyclones and anticyclones and transient waves in the westerlies. Throughout this paper, the term "modes" refers to one of the four circulation mechanisms defined in eq (4), whereas the term "synoptic feature" will be used to designate individual synoptic wave patterns.

3. DATA AND METHOD OF ANALYSIS

The energy transport calculations were carried out using a spherical grid that covered most of the North American continent (fig. 1). Within this region, there is a total of 90 radiosonde stations. An additional 15 stations outside the region were included for computing the parameters near the boundary. By means of an objective analysis computer program, data from radiosonde stations were extrapolated to a grid with a horizontal resolution of 2.5° latitude-longitude and a vertical resolution of 50 mb between the surface and 100 mb. The effects of variation in surface topography and surface pressure at each radiosonde station were taken into account by weighting the transport in the lowest layer according to the difference between the surface pressure and the pressure at the top of the 50-mb interval above the surface. Using the above grid, the minimum detectable scale is approximately 5°. The program analyzed five parameters: the u- and v-wind components, temperature, relative humidity, and geopotential height. The details of the analysis are described by Astling (1970). The basic concept of the objective analysis technique was similar to one described by Cressman (1959).

The meridional fluxes of the four energy forms by each circulation mode were calculated for 0000 and 1200 GMT each day. The values were averaged with respect to time and longitude to produce 1- and 3-mo averages. In addition, daily values of transient eddy fluxes at individual gridpoints on one lower (700-mb) and one upper level (250-mb) pressure surface were studied for use in some synoptic case studies.

The months of January, February, and March 1966 were selected because several distinct large-scale circulation features developed or moved over North America during this period, permitting an examination of the energy transport associated with several types of large-scale atmospheric patterns. For example, during March, two situations occurred where a deep closed Low at upper levels developed over the central United States. In the other 2 mo, large-amplitude trough and ridge systems were frequently present. In addition, the classical pattern of an index cycle took place over the western half of the Northern Hemisphere in January and Februray 1966 (Posey 1966, Green 1966).

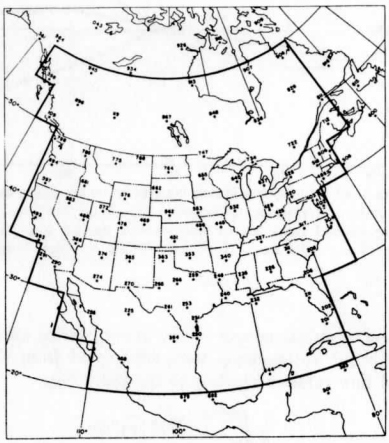

FIGURE 1.—The data region (outlined by a heavy line) and the location of radiosonde stations used in this study.

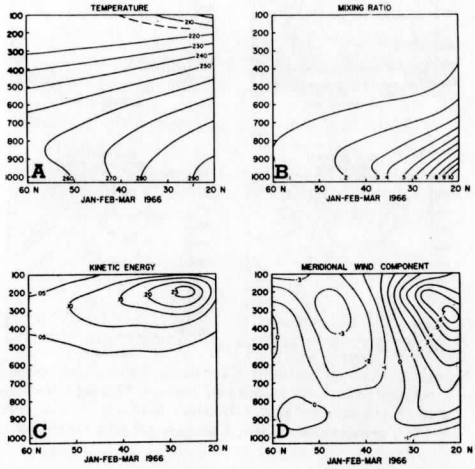

FIGURE 2.—Time- and longitude-averaged values, (A) temperature (°K), (B) mixing ratio (g/kg), (C) kinetic energy (cal/g), and (D) meridional wind component (m/s) for January, February, and March 1966.

4. AVERAGES OF THE POLEWARD ENERGY TRANSPORT

Before discussing the poleward energy transport by the four circulation modes, it is helpful to note the general character of the circulation patterns and distribution of the energy parameters that existed over the North American region during the period of study.

The time- and longitude-averaged values of the four parameters used in calculating energy fluxes are shown in figure 2. The distribution of temperature is very similar to the temperature distribution for the entire Northern Hemisphere (fig. 2A) For example, at most latitudes, the temperatures obtained here for North America were within 2°C of the hemispheric averages obtained by Starr and Wallace (1964). The north–south temperature difference at 1000 mb is 35°C between latitudes 20° and 60°N, while at 100 mb the gradient is reversed and amounts to 15°C.

Figure 2B reveals, as expected, that the moisture is concentrated below the 700-mb level with the largest amounts at 20°N. The horizontal gradient of moisture and, thus, latent heat is very large compared to the gradient of sensible heat. Obviously, surface cyclones and anticyclones, as well as surface terrain features, strongly influence the moisture transport.

The vertical distribution of kinetic energy for January, February, and March 1966 (fig. 2C) indicates that the average position of the jet stream was located near 27°N during the data period. This position is somewhat south of the climatic mean 300-mb position of the jet stream over this region as indicated by Lahey et al. (1960).

Figure 2D shows that, for the 3-mo period, the mean meridional wind component was northerly (negative) throughout the troposphere and lower stratosphere poleward of 32°N. The mean circulation over North America during this time was characterized by a trough over the eastern portion of the area with a ridge in the west producing the northerly flow (Posey 1966, Green 1966, Stark 1966). Comparisons with the mean surface resultant winds prepared by Bryson (1966) indicate that the region of confluence associated with the Pacific front was displaced south of its mean position over the midwestern United States during the period of study. The mean meridional wind component equatorward of 32°N was characterized by strong southerly flow in the upper troposphere and weak northerly flow near the surface. Although the equatorward moving branch was not well developed, the pattern, in general, is that associated with the Hadley cell. Except for the intensity of the flow, the pattern presented in figure 2D is in qualitative agreement with the time-averaged pattern obtained by Palmén and Vuorela (1963).

a. Mean Meridional Circulation

The vertical and latitudinal distributions of the energy transports by the mean meridional circulation for the North American sector as calculated from eq (4) are presented in figure 3. Equatorward of about 32°N, the net transport of both sensible heat and geopotential energy for the surface to 100-mb layer was toward the north. At these latitudes, the transport of *both* energy forms by the high-level northward moving branch of the Hadley circulation was much greater than that accomplished by the low-level southward moving branch (figs. 3A, 3D). Poleward of 32°N over the North American sector, the transports of sensible heat and geopotential energy were mainly southward, with the high-level south-

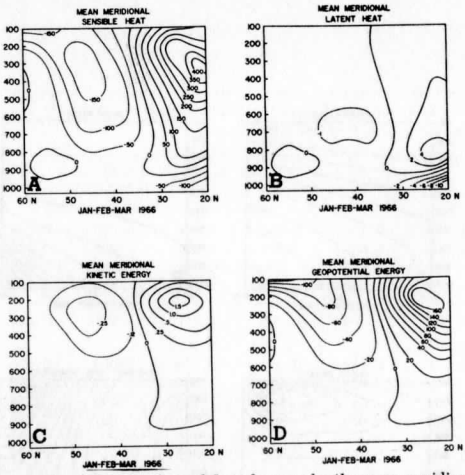

FIGURE 3.—Average poleward flux of energy by the mean meridional circulation over North America for January, February, and March 1966 of (A) sensible heat, (B) latent heat, (C) kinetic energy, and (D) geopotential energy. Units are 10^2 cal·s^{-1}·mb^{-1}·cm^{-1}.

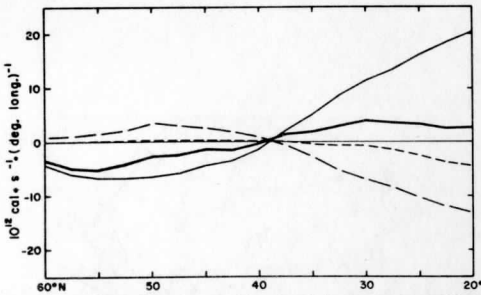

FIGURE 4.—Vertically integrated transports by the mean meridional circulation of geopotential energy (thin solid line), sensible heat (long dashed line), latent heat (short dashed line), and their sum (heavy solid line). Units are 10^{12} cal·s^{-1}·(deg. long.)$^{-1}$.

ward moving branch of the Ferrel circulation being dominant.

In general, the transports by the mean meridional circulation for the North American sector were much larger than those calculated by Holopainen (1965) and Oort (1971*a*), being nearly two orders of magnitude larger at some latitudes. The large values were principally the result of strong meridional wind speeds and a tendency for the existence of very weak compensating flow between high and low elevations over North America.

Because of the large transport estimates, the question might be raised as to whether a mean meridional transport calculated in this way for a limited area has significance. The authors feel that it does, for it provides a quantitative estimate of the large longitudinal variations that exist in the intensity of the meridional circulations. Moreover, the insufficient compensating motion in the mean meridional circulation over North America emphasizes the basic helical nature of meridional overturnings. The longitudinal variations do not consist simply of more intense overturnings in a north–south plane at some longitudes than others, but rather represent large poleward transports at high levels for some longitudes with the tendency for low-level compensating motion to occur at other longitudes.

Although the mean meridional transport estimates, as calculated from eq (4), point out some of the often neglected characteristics of the north–south overturnings, the large values make comparisons with the estimates obtained for the other three modes of circulation difficult. Consequently, a second method was used to calculate the mean meridional fluxes for the North American sector following a suggestion by Oort (1971*b*). The vertical mean component of the energy terms and meridional wind components were subtracted from the computed flux values according to the following:

$$\frac{1}{g}\int_{p_0}^{100\text{ mb}} \{\overline{E}\}''\{\bar{v}\}'' dp \tag{5}$$

where

$$\{E\}'' = \{E\} - \int_{p_0}^{100\text{ mb}} \{E\} dp/(p_0 - 100). \tag{6}$$

A similar expression was used for $\{v\}''$.

With this new definition, the transports calculated for the mean meridional circulation were two orders of magnitude smaller than the estimates obtained from $\{\overline{E}\}\{\bar{v}\}$. From the results illustrated in figure 4, one can see that the net transport was northward between 20°N and approximately 38°N latitude and amounted to approximately 3×10^{12} cal·s^{-1}·(deg. long.)$^{-1}$. In this region, the geopotential and sensible heat terms were dominant, with northward transport by the Φ term partially canceling the southward flow of sensible heat. In contrast, north of 38°N, each energy term contributed much less to the mean meridional fluxes, and the net transport was directed southward. These estimated transports are larger than the transports by eddy circulations in southern latitudes (discussed in the next section) but are smaller in middle latitudes and agree with the results obtained by Oort (1971*a*) and Holopainen (1965).

b. Transient Eddies

The results of the energy transport calculations of the transient eddy, standing eddy, and transient meridional circulations are listed in table 1. At all latitudes but 20°N, the transient eddy circulation was the dominant transport mechanism among the remaining circulation modes, with the sensible and latent heat fluxes being dominant. Poleward fluxes were largest in the middle latitudes, where the transient eddy mode contributed approximately three-fourths of the total poleward transport by the modes in-

TABLE 1.—*Average transport of sensible and latent heat and geopotential and kinetic energy over North America for January, February, and March 1966 by transient eddies, standing eddies, and transient meridional circulation. Values represent the poleward transport across latitudes at 5° intervals between the surface and 100 mb. Units are* 10^{12} *cal* $\cdot s^{-1} \cdot$ *(deg. long.)*$^{-1}$.

Mode/Latitude	60°N	55°	50°	45°	40°	35°	30°	25°	20°N
Transient eddy									
c_pT	0. 569	0. 736	1. 292	1. 794	2. 103	1. 933	1. 286	0. 525	0. 008
Lq	. 119	. 214	0. 356	0. 506	0. 628	0. 922	1. 047	. 936	. 339
ϕ	−. 039	−. 125	−. 072	. 042	. 053	. 031	−0. 047	−. 122	−. 069
(V•V)/2	−. 011	−. 047	−. 031	−. 003	. 050	. 083	. 111	. 142	. 067
Total	0. 638	0. 778	1. 545	2. 339	2. 834	2. 969	2. 337	1. 481	0. 345
Standing eddy									
c_pT	−0. 164	0. 339	0. 531	0. 386	0. 153	0. 094	0. 378	0. 089	−0. 030
Lq	. 028	. 169	. 222	. 100	. 028	. 081	. 206	. 197	−. 292
ϕ	. 028	−. 056	−. 089	−. 044	−. 081	−. 017	−. 136	. 044	. 039
(V•V)/2	−. 008	−. 008	−. 003	. 017	. 053	. 097	. 080	. 022	. 006
Total	−0. 172	0. 444	0. 661	0. 459	0. 153	0. 252	0. 809	0. 352	−0. 277
Transient meridional									
c_pT	0. 269	0. 342	0. 133	0. 100	0. 361	0. 317	0. 378	0. 364	0. 194
Lq	. 094	. 050	. 039	. 081	. 139	. 156	. 342	. 297	. 214
ϕ	. 047	−. 008	−. 067	−. 044	. 003	−. 014	−. 036	−. 025	. 028
(V•V)/2	−. 011	−. 019	. 000	. 031	. 042	. 039	. 047	. 047	. 019
Total	0. 399	0. 365	0. 105	0. 168	0. 545	0. 498	0. 731	0. 683	0. 455
Grand total	0. 865	1. 587	2. 311	2. 966	3. 532	3. 719	3. 877	2. 516	0. 523

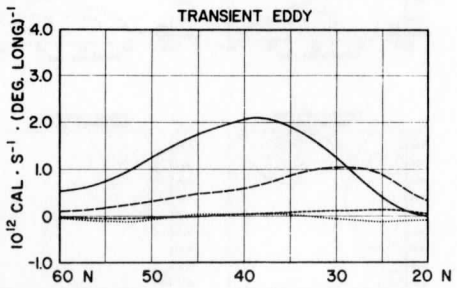

FIGURE 5.—Mean poleward flux of sensible heat (solid line), latent heat (long dashed line), kinetic energy (short dashed line), and geopotential energy (dotted line) over North America by transient eddy circulations for January through March 1966. Units are 10^{12} cal $\cdot s^{-1} \cdot$ (deg. long.)$^{-1}$.

volving transient and eddy circulations. In figure 5, the transient eddy fluxes for the four energy forms are presented graphically. The flux of sensible heat reached a maximum of 2.2×10^{12} cal $\cdot s^{-1} \cdot$ (deg. long.)$^{-1}$ at 37.5°N. On the other hand, the flux of latent heat was largest south of this latitude, reaching a value of 1.0×10^{12} cal $\cdot s^{-1} \cdot$ (deg. long.)$^{-1}$ at 30°N. The difference between the latitudes of maximum flux of sensible heat and latent heat is likely associated with the occurrence of cyclones along the polar front. In North America for the winter season, the mean latitude of the polar front is between 35° and 40°N, and it is at these latitudes that the sensible heat flux is a maximum. The moisture source for cyclones over the eastern one-half or two-thirds of the continent is the Gulf of Mexico, Caribbean Sea, and warm Atlantic adjacent to the Southeastern States. As moist air moves northward ahead of the migratory (and often occluding) cyclones and dry air moves southward to the rear, a maximum gradient of moisture and flux is typically found to the south of the cyclone track. The vertical distribution of the average poleward energy flux by transient eddies for January through March 1966 is shown in figure 6 for each of the energy terms.

Note that near the tropopause in low latitudes the kinetic energy fluxes were the largest of the four transport energy terms, exceeding 0.6×10^2 cal$\cdot$s$^{-1}\cdot$mb$^{-1}\cdot$cm^{-1} at 25°N near 200 mb. Kinetic energy fluxes for individual months were a maximum at upper levels in the vicinity of the jet stream where the kinetic energy was largest. In February, for example, the poleward fluxes were largest at the tropopause level between 20° and 40°N, where the winds were much stronger than in either January or March 1966. In studies of the poleward transport of energy at high levels, the kinetic energy flux should not be ignored.

c. Standing Eddies

An examination of figure 7, which depicts the vertical and latitudinal variations of the standing eddy fluxes, reveals that near 50°N fluxes of sensible and latent heat amount to 2 and 1.25×10^2 cal$\cdot$cm$^{-1}\cdot$s$^{-1}\cdot$mb^{-1}, respectively. The relatively large fluxes at 50°N may be the result of a strong, standing eddy circulation associated

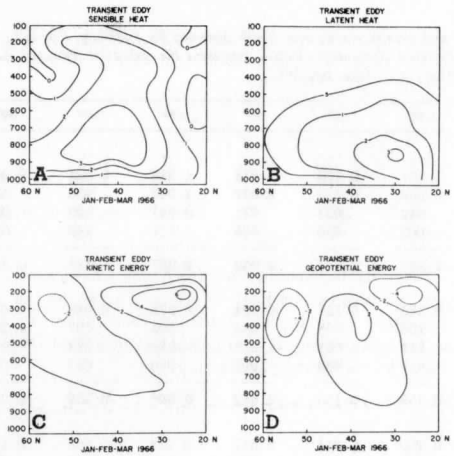

FIGURE 6.—Time- and longitude-averaged poleward energy transport of (A) sensible heat, (B) latent heat, (C) kinetic energy, and (D) geopotential energy by transient eddies. Units are 10^2 cal $\cdot s^{-1} \cdot mb^{-1} \cdot cm^{-1}$.

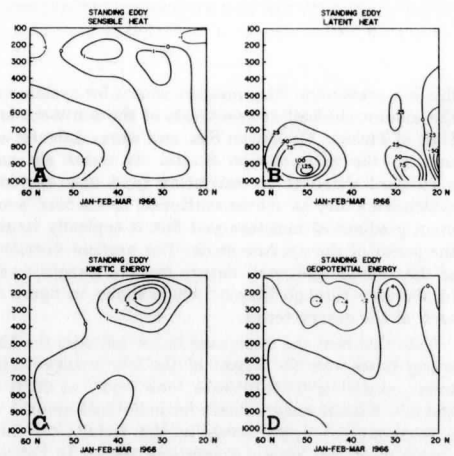

FIGURE 7.—Same as figure 6 for transport by standing eddies.

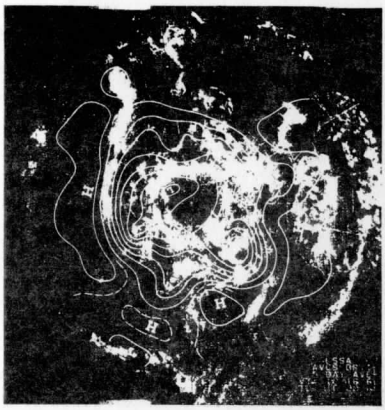

FIGURE 8.—Five-day (Oct. 16–20, 1968) average cloud brightness picture from ESSA 7 with the corresponding 5-day mean 700-mb height contours superimposed (Andrews 1969).

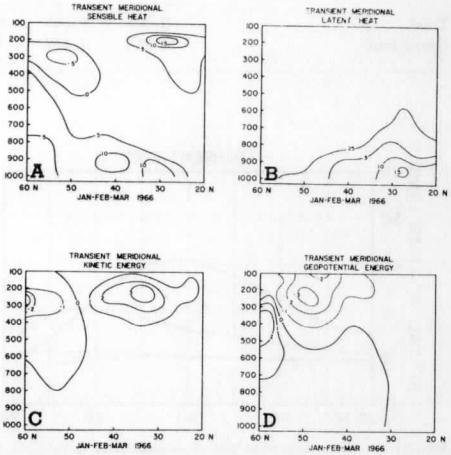

FIGURE 9.—Same as figure 6 for transport by transient meridional circulations.

with the Aleutian Low. A strong southwesterly flow of relatively warm, moist air enters the region along the Northwest Pacific Coast of the continent. The secondary maximum of standing eddy latent heat flux noted at latitudes 25° to 30°N is accomplished primarily by quasi-stationary subtropical anticyclones. An example of this circulation mode is illustrated in figure 8, which shows a 5-day mean 700-mb height field superimposed on an ESSA 8 cloud brightness map of the Northern Hemisphere for Oct. 16–20, 1968. The extensive areas of cloudiness present in the flow around the west side of the subtropical high are especially evident between 25° and 30°N over the central Atlantic and eastern United States.

The standing eddy flux of latent heat at 20°N was the only circulation mode of the three shown in figures 6B, 7B, and 9B in which the net transport of latent heat was directed equatorward. For this circulation mode, an apparent region of moisture divergence was present near 22°N with southward transports on the equatorward side and northward transports on the poleward side. Adem (1968), in a study of the atmospheric water budget for the whole Northern Hemisphere for one winter season, found that standing eddy fluxes of moisture were large and directed equatorward at low latitudes. Hastenrath

TABLE 2.—*Comparison of the average transient eddy flux of total energy as calculated by Oort (1971a) for the 3 mo of January, February, and March (5 yr of data) with the equivalent flux calculated for the North American sector for January–March 1966. Oort's figures are for the surface to 75 mb; those for North America are for the surface to 100 mb. Units are* 10^{12} *cal·s*$^{-1}$*·(deg. long.)*$^{-1}$.

	60°N	55°	50°	45°	40°	35°	30°	25°	20°N
Northern Hemisphere (Oort)	1. 200	1. 425	1. 597	1. 843	2. 122	2. 326	2. 079	1. 415	0. 652
North America	1. 037	1. 143	1. 650	2. 507	3. 279	3. 467	3. 068	2. 164	0. 800

(1966) found an export of latent heat from the Gulf of Mexico.

The standing eddy flux of kinetic energy in figure 7C is similar to the flux by transient eddies with maximum values near 200 mb and 32°N (fig. 6C). The large poleward flux values are probably associated with the large-scale trough over the United States. An examination of standing eddy fluxes of kinetic energy at individual gridpoints indicated that the maximum poleward fluxes occurred along the northern edge of the jet stream which was located over Mexico and the southeastern United States. The export of kinetic energy from the jet core maximum by the standing eddy flux is not characteristic of the concept of eddies supplying energy to the mean flow.

The standing eddy flux of geopotential energy (fig. 7D) is largest in the levels above 300 mb with values similar to the transient eddy flux of geopotential energy. Although the geopotential energy fluxes are small, they indicate the presence of nongeostrophic motions since no geopotential energy flux would exist if the flow was geostrophic. As pointed out by Godson (1950), the difference between the actual and geostrophic wind speed is largest for speeds exceeding 25 m/s. Consequently, large fluxes of geopotential energy should be expected at higher levels. Positive fluxes would be associated with subgeostrophic winds in southward flow and supergeostrophic winds in northward flow of a stationary eddy.

d. Transient Meridional Circulations

An examination of table 1 reveals that the total energy fluxes accomplished by the transient meridional circulation were largest at 25°–30°N. This latitudinal region is the transition zone between the Hadley circulation in the tropical latitudes and the circumpolar vortex in middle and polar latitudes. It is likely that the expansion and contraction of the meridional circulation system would produce the large transient fluxes in this latitude zone. In figure 9, the fluxes of sensible heat and kinetic energy at high levels and latent heat at low levels appear to be responsible for the maximum at 25° and 30°N.

e. Comparisons With Other Studies

An advantage in studying the energy transport for a limited longitudinal sector is that statistics obtained for the sector can be compared with statistics based on hemispheric wide studies to describe significant longitudinal variations in the modes of the transport. In this section, we turn to a comparison of the circulations involving space and time deviations obtained for North America with the excellent results obtained by Oort (1971*a*) for an area completely encircling the Northern Hemisphere. In making the comparison, it is important to note that Oort employed the following partitioning:

$$\{\overline{\Pi}_i\}=\{\overline{E}_i\}\{\bar{v}\}+\{\overline{E}_i^*\bar{v}^*\}+\{\overline{E_i'v'}\}, \tag{7}$$

while in this study,

$$\{\overline{\Pi}_i\}=\{\overline{E}_i\}\{\bar{v}\}+\{\overline{E}_i^*\bar{v}^*\}+\overline{\{E_i\}'\{v\}'}+\{\overline{E_i'^*v'^*}\} \tag{8}$$

where $\{\overline{\Pi}_i\}$ is the time- and longitude-averaged transport of one energy form for a 1-mb layer. Thus the last term in eq (7), which Oort labels the "transient eddy" mode, is equivalent to the sum of the transient eddy and transient meridional modes calculated here; that is,

$$\{\overline{E_i'v'}\}=\overline{\{E_i\}'\{v\}'}+\{\overline{E_i'^*v'^*}\}. \tag{9}$$

Equation (9) has been used to equate the transient eddy term calculated by Oort (1971*a*) with the equivalent estimates obtained in this study (table 2). Oort's January, February, and March mean monthly values (based on 5 yr of data) for the Northern Hemisphere have been averaged to provide a comparison with the means for the 3-mo period (January–March 1966) of this study. Both sets of data are for the total energy and are expressed in units of 10^{12} cal·s^{-1}· (deg. long.)$^{-1}$. One should remember that Oort's figures represent a 5-yr average, while those in this study involve only 1 yr.

Since the transient eddy mode involves synoptic scale size features, the truncations that result from using a limited longitudinal sector are not severe. In table 2 there is good agreement between the statistics for the Northern Hemisphere and those for North America. In both sets, the maximum transport occurs at 35°N but with the North American sector having a 50-percent greater value. Since the North American area tends to be a region with vigorous cyclone development and since the early part of 1966 was a period of unusual cyclonic activity, the larger figure was expected. It is interesting to note that the latitudinal variation of flux is distinctly larger over North America than for the hemisphere. In fact, at 55°–60°N, the hemispheric values exceed those for North America. Over North America, the mean winter position of the jet stream, and the associated storm track, is displaced somewhat farther south than in the eastern Atlantic, Eurpoean, and eastern Pacific sectors. Thus, if one does hemispheric averaging, the flux of energy by transient features will show a smoother latitudinal profile than for a single sector.

TABLE 3.—*Same as table 2 for the standing eddy mode*

	60°N	55°	50°	45°	40°	35°	30°	25°	20°N
Northern Hemisphere (Oort)	1. 083	1. 522	1. 704	1. 458	0. 943	0. 579	0. 386	0. 300	0. 214
North America	−0. 172	0. 444	0. 661	0. 459	0. 153	0. 256	0. 809	0. 352	−0. 277

An examination of a breakdown of the total energy flux by the transient eddy mode into the four energy forms reveals that, both for North America and the Northern Hemisphere, the sensible heat flux was largest, and the maximum flux was at 40°N. In the case of the latent heat flux, both studies obtained a maximum at 30°N; however, for the Northern Hemisphere, the value at this latitude exceeded the value for sensible heat, while for the continental sector of North America the flux of latent heat was slightly less than that of sensible heat. Over North America, the variation in the latent heat flux between 30° and 60°N amounted to a factor of more than eight, while for the Northern Hemisphere the factor was only about four, which again emphasizes the sharper latitudinal variations in North America. In both studies, the flux of geopotential energy was quite small and generally negative. The flux of kinetic energy was also small in both studies.

Table 3 provides a comparison of the standing eddy flux of the total energy for North America with Oort's values for the Northern Hemisphere. The most noteworthy difference between the two sets of statistics is the considerably greater transport by the standing eddy mode for the Northern Hemisphere latitudes north of 40° or 45°N. The large standing eddies associated with features such as the Aleutian and Icelandic Lows, which are truncated when only the North American sector is studied, appear to be responsible for this greater transport. In looking at the breakdown of the transport into each of the four energy forms (table 4 in Oort's paper and table 1 in this paper), the large transport of sensible heat by the standing eddies averaged around the higher latitudes of the hemisphere stands out. As Oort (1971*a*) points out, the standing eddies rather than the transient eddies appear to accomplish the bulk of the transport of sensible heat at higher latitudes. Although the North American data does not support this observation, the truncations that exist in using the limited sector may well obscure the large transport.

5. IMPORTANCE OF VARIOUS LARGE-SCALE SYNOPTIC WEATHER SYSTEMS

Since the transient eddy circulations involve waves of various lengths and shapes, the question arises as to which eddies are most effective in the poleward transport. In calculating the transport associated with various wave numbers, Wiin-Nielsen et al. (1963) found that wave numbers ≤ 4 were responsible for approximately 45 percent of the sensible heat transport while wave numbers 6–8 accounted for 40 percent of the transport at 40°N, the middle latitude of the area studied here. However, as Barrett (1961) has pointed out, wave shape has been neglected or considered as secondary in importance in the transport. In this paper, the role of wave shape has been investigated for wave numbers 6–9 (i.e., wavelengths between 40° and 60° of long.). Because of the limited longitudinal sector, smaller wave numbers could not be analyzed, however, from baroclinic instability theory, wave numbers around 6 are quite active and are thus of interest.

a. Selection of Synoptic Features

In examining the eddy transport associated with wavelengths between 40° and 60° of longitude, one encounters the problem of which pressure level should be used in defining the wave pattern. The 500-mb surface was chosen as being the most representative, but the transports were calculated for the 700- and 250-mb levels. Winston (1961) found that the energy transport for the 850- to 500-mb layer is well correlated with the transport for the entire troposphere. The 700-mb surface was chosen as representative of the 850- to 500-mb layer while the transport at 250 mb was chosen to represent the high levels. Because of the relative importance of the various energy terms, only the sensible heat and latent heat are discussed for the 700-mb surface, the discussion of the fluxes at 250 mb are confined to sensible heat, geopotential energy, and kinetic energy.

For the 3-mo period of study, a total of 20 cases were selected and divided into five types of synoptic features based on the 500-mb geopotential height field. Included were two types of large-scale trough systems, a closed Low, a large-scale ridge, and a zonal flow pattern, all of which are characteristic of middle latitude synoptic weather systems. The five synoptic features and the criteria used in selecting them were:

1. Closed Low—an upper level Low center in which there were two or more closed contours in the 500-mb height field.
2. Open wave trough—a trough in which the wave amplitude (defined as the distance between the northern and the southernmost positions of a given contour line) of the 500-mb height contours was greater than 15° of latitude and the trough axis intersected the central meridian by an angle of less than 10°.
3. Eastward tilting trough—a trough in which the amplitude of the 500-mb height contours was greater than 15° of latitude and the trough axis intersected the central meridian by an angle greater than 20°.
4. Ridge—a ridge in which the wave amplitude of the 500-mb height contours was greater than 15° of latitude and the ridge axis intersected the central meridian by an angle of less than 10°.
5. Zonal flow—the contour pattern over at least a 10° latitude zone was nearly parallel to the latitude circles, any wave present having an amplitude of less than 5° latitude.

Examples of the types of cases used in this study are shown in figure 10. Five cases satisfied the criteria for

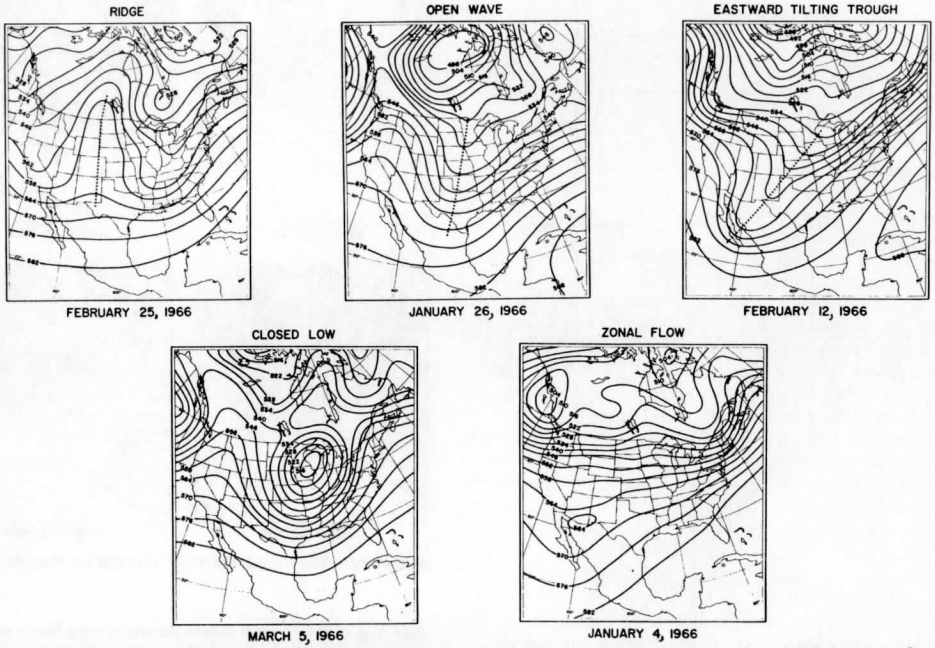

FIGURE 10.—Examples of the five synoptic features listed in table 5. Solid lines are 500-mb contours and are labeled in tens of meters. Dotted lines represent trough and ridge axes.

each of the first three types. Two cases satisfied the criteria for the ridge type, and three cases fulfilled the zonal flow criteria for a portion of the region of study. All of the selected cases occurred on nonconsecutive days. The first three synoptic features had wavelengths of approximately 40°–60° of longitude (i.e., wave no. 6–9) while the cases that satisfied the fourth had wavelengths of approximately 40° of longitude.

b. Composite Fluxes

For the open waves and eastward tilting troughs, composite averages of the eddy fluxes were obtained at 2.5° grid intervals using the trough axis as a reference line. Similarily, composite averages were obtained for the closed Low circulation type except that the Low center was used as the reference point.

Composite 700- and 250-mb averages for the latitude of maximum transport for each of the synoptic features are listed in table 4. At both elevations, the closed Low is decidedly the most effective feature in the poleward transport. The energy transport associated with the open wave is only about one-half that produced by the closed Low. The eastward tilting trough, which is an essential mechanism in the poleward transport of eastward momentum, is quite ineffective in the poleward transport of energy, at least in the small sample of cases studied here. Except for a sizable transport of sensible heat at 250 mb, the ridge and zonal flow features contributed little to the transport.

TABLE 4.—*Composite average of the poleward flux of energy at the latitude of maximum transport accomplished by the five synoptic features. Units are* 10^2 *cal·s*$^{-1}$*·mb*$^{-1}$*·cm*$^{-1}$.

Feature	700 mb		250 mb		
	c_pT	Lq	c_pT	ϕ	$V^3/2$
Closed Low	12.3	4.7	7.9	2.2	0.7
Open wave	6.6	2.1	5.1	−0.9	1.0
Eastward tilting trough	0.4	1.2	−2.9	−1.2	1.3
Ridge	−1.4	1.0	9.0	−1.7	−0.2
Zonal flow	1.4	0.5	0.8	−0.3	0.6

The composite energy flux averages accomplished by the closed Low are shown in figure 11. The Low center is represented by the intersection of the coordinate axes, and the grid spacing from the center is marked for every 5°. At 700 mb, an area of large transport of sensible heat was located to the east of the Low and another to the west, with the maximum value of 30×10^2 cal·s^{-1}·mb^{-1}·cm^{-1} located between 5° and 10° west of the Low. Similar sensible heat flux values were found at 250 mb; however, because of the westward tilt of Lows with respect to height, the maximum flux of sensible heat at 250 mb was displaced westward. In contrast, the flux of latent heat

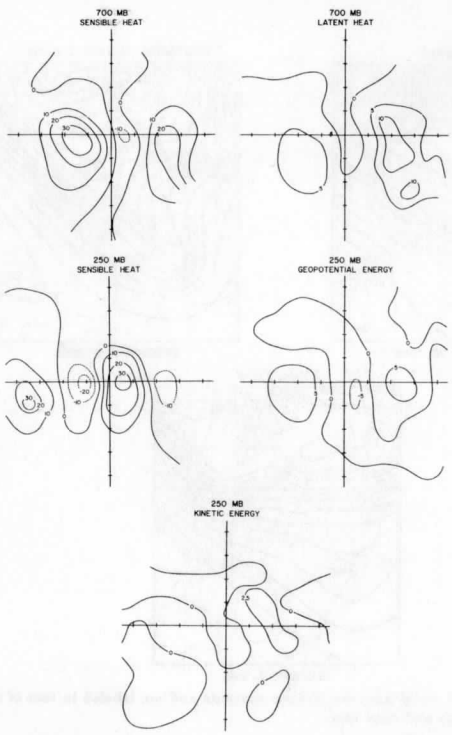

FIGURE 11.—Composite averages of the energy fluxes accomplished by the closed Low synoptic features at 700 and 250 mb. Distances from the Low center are marked at grid intervals of 5°. Units are 10^2 cal $\cdot s^{-1} \cdot mb^{-1} \cdot cm^{-1}$.

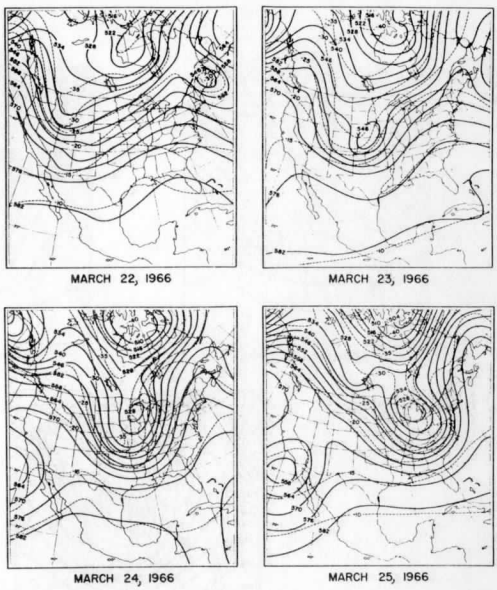

FIGURE 12.—The 500-mb charts for 0000 GMT on Mar. 22–25, 1966.

was large only to the east of the Low, with values of 10×10^2 cal $\cdot s^{-1} \cdot mb^{-1} \cdot cm^{-1}$ at 700 mb. Small flux values of geopotential and kinetic energy were present at 250 mb. In all cases, the areas of maximum fluxes were separated by an elongated area of small negative fluxes that extended north–south through the Low center.

The significance of the energy fluxes accomplished by closed Low synoptic features is evident when a comparison is made with the average fluxes by transient eddies in middle latitudes as shown in figure 6. The maximum fluxes of the four energy forms across the latitude that intersects the closed Low center are nearly 10 times as large as the longitude-averaged poleward energy transport at both 700 and 250 mb. Moreover, the average energy flux across the center latitude of the closed Low is approximately five times larger than the transient eddy flux shown in figure 6. If we assume that the 3-mo averaged fluxes by transient eddies are representative of the hemisphere as a whole, two intense closed Lows present in middle latitudes could account for the poleward fluxes by transient eddy circulations. Because the transient flux (per deg. of long.) over North America very likely exceeded that for the whole hemisphere, the effectiveness of the transport by the closed Low feature is all the more impressive. The importance of closed Lows in transporting energy is not surprising when one notes that Palmén (1959), for example, estimated that a closed Low associated with a well-developed extratropical cyclone produced enough kinetic energy to balance the frictional dissipation for the entire Northern Hemisphere poleward of latitude 30°N.

c. A Case Study

Because of the large energy fluxes accomplished by closed Lows, a more detailed study was made of the fluxes associated with the evolution of one such system. Figure 12 presents a sequence of 500-mb charts for the period Mar. 22–25, 1966. The system began to develop early on March 22 when a trough system moved from the Pacific into the western United States. Within 24 hr, the trough had deepened and a closed 500-mb Low appeared over Nebraska. During the next 2 days, the closed Low intensified as it moved eastward.

The daily transient eddy fluxes of sensible and latent heat at 700 mb are presented in figures 13 and 14. During the first day, the flux of sensible heat was moderate. It increased on the second day, reached a maximum on the third day, and decreased slightly on the fourth day. Although the flux of latent heat was less, it did reach 40 percent of the sensible heat flux on the last 2 days when the system had moved far enough to the east to tap the

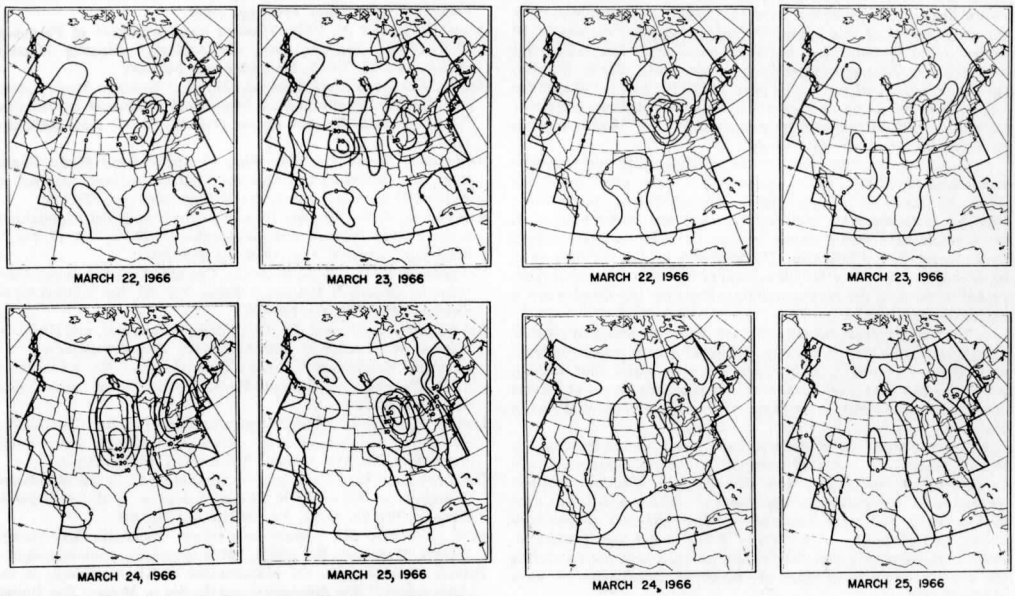

FIGURE 13.—Transient eddy fluxes of sensible heat at 700 mb for 0000 GMT on Mar. 22–25, 1966. Units are 10^{12} cal $\cdot s^{-1} \cdot mb^{-1} \cdot cm^{-1}$.

FIGURE 14.—Same as figure 13 for latent heat.

TABLE 5.—*Values of the maximum transports of sensible and latent heat at 700 mb for areas west and east of the 500-mb closed Low center. Units are* 10^{2} *cal* $\cdot s^{-1} \cdot mb^{-1} \cdot cm^{-1}$.

Date (1966)	Time (GMT)	Sensible heat		Latent heat	
		West of Low center	East of Low center	West of Low center	East of Low center
Mar. 22	0000	23	23	16	12
	1200	30	23	9	11
23	0000	34	25	5	7
	1200	45	48	8	31
24	0000	41	37	9	21
	1200	40	37	12	34
25	0000	34	28	11	25

moisture sources of the Gulf of Mexico and the Atlantic Ocean. Table 5 summarizes the maximum transport of sensible and latent heat to the west and east of the Low center during the 4-day period.

An examination of the 500-mb charts (fig. 12) reveals that, as expected, the greatest transport of sensible heat occurred on March 24 when the temperature and pressure fields were most out of phase. It is well known that developing baroclinic disturbances with their out-of-phase relationship combined with an increasing meridional flow produce large transports of heat. Haines and Winston (1963) found that the greatest poleward flux of sensible heat occurs in the regions east of the Asian and North American continents. Both are regions in which there are frequent developments of baroclinic waves. Wiin-Nielsen et al. (1963) found that the ultralong waves (wave no. 1–3) are responsible for a major portion of the poleward heat transport. Wave number 3, for example, is typically associated with troughs off the east coast of North America and Asia. The results obtained in the case studied here suggest that the sensible heat transport is mainly associated with the development of smaller scale baroclinic disturbances that are imbedded in the ultralong waves in these areas.

6. SUMMARY

The study of the poleward transport of four forms of energy by four modes of circulation for the winter of 1966 over North America was undertaken to provide estimates of the transport based on an excellent network of radiosonde stations and to permit an examination of the particular contribution the North American sector makes toward the hemispheric transport. The more noteworthy results include:

1. Two computational methods were carried out for the mean meridional circulation. In one method, very large poleward transports of sensible heat and geopotential energy occurred in southern latitudes at high levels. The large values point to large longitudinal variations in the meridional overturnings and suggest a helical structure to the meridional circulation. In the second computational method, vertical mean components were subtracted from the energy terms and the meridional wind component. The results indicated transport values within an order of magnitude of the flux values by other circulation modes. Poleward fluxes occurred in the southern latitudes, where the Hadley circulation is dominant, and weak southward fluxes occurred in middle and northern latitudes.

2. Of the remaining three modes, the transport eddy was dominant. The total energy transport by transient eddies was a maximum near 35°N, in agreement with Oort's (1971*a*) figures for the entire hemisphere. However, over the North American sector for the data period of this study, the maximum flux was nearly 50 percent greater than that for the hemisphere. The latitudinal variation of the transient eddy transport over North America showed a considerably sharper peak at 35°N than for the entire hemisphere indicating that there is a somewhat more restricted latitudinal belt of frequent transient eddies over North America than for the hemisphere as a whole.

3. Energy fluxes calculated by the standing eddy and transient meridional circulation modes amounted to only one-fifth of the fluxes by transient eddies. These two circulation modes were effective in transporting only sensible heat and latent heat, with the sensible heat fluxes largest in high latitudes and latent heat fluxes largest in low latitudes. The transport by the standing eddy mode was less than Oort's (1971*a*) values for the whole hemisphere probably because the large standing eddies are truncated when a limited area is studied.

4. In most previous studies, only sensible heat and geopotential energy were considered; the flux of kinetic energy was considered as negligible. However, in this study it was found that at high levels the transient meridional and standing eddy fluxes of kinetic energy were frequently of the same order as the geopotential energy transport.

5. Wave shape was of definite importance in determining the effectiveness of the poleward transport of energy. Large amplitude troughs with closed Low centers were the most effective transport mechanisms, accomplishing large fluxes of sensible and latent heat at low levels and large fluxes of sensible heat and geopotential energy at high levels. A case study of one closed Low feature revealed, as expected, that the maximum transport occurs during the rapidly intensifying stage of baroclinic disturbances of wave numbers 6–9.

ACKNOWLEDGMENTS

The authors are grateful to Abraham Oort for his helpful suggestions and to Peter Guetter for developing the computer programs.

This research was supported by the National Environmental Satellite Center, ESSA (now NOAA) under grants WBG–52 and E–8–69 (G). Acknowledgment is also made to the University of Wisconsin Alumni Research Foundation for providing computer unds to develop the computer programs at the University of Wisconsin Computing Center and to the National Center for Atmospheric Research, which is sponsored by the National Science Foundation, for use of its Control Data Corporation 6600 computer to process the data.

REFERENCES

Andrews, James F., "The Circulation and Weather of 1968," *Weatherwise*, Vol. 22, No. 1, Feb. **1969**, pp. 5–11.

Adem, Julian, "A Parametric Method for Computing the Mean Water Budget of the Atmosphere," *Tellus*, Vol. 20, No. 4, Stockholm, Sweden, July **1968**, pp. 621–631.

Astling, E. G., "A Study of Atmospheric Energy Transports Over North America," Ph. D. thesis, Department of Meteorology, University of Wisconsin, Madison, Jan. **1970**, 101 pp.

Barrett, Earl W., "Some Applications of Harmonic Analysis to the Study of the General Circulation, Pt. 1: Harmonic Analysis of Some Daily and Five-Day Mean Hemispheric Contour Charts," *Beiträge zur Physik der Atmosphäre*, Vol. 38, No. 3/4, Vieweg & Sohn, Frankfurt a.M., Mar. **1961**, pp. 280–322.

Bryson, Reid A., "Airmasses, Streamlines, and the Boreal Forest," *Geographical Bulletin*, Vol. 8, No. 3, Mar. **1966**, pp. 228–269.

Cressman, George P., "An Operational Objective Analysis System," *Monthly Weather Review*, Vol. 87, No. 10, Oct. **1959**, pp. 367–374.

Godson, Warren Lehman, "A Study of the Deviations of Wind Speeds and Deviations From Geostrophic Values," *Quarterly Journal of the Royal Meteorological Society*, Vol. 76, No. 327, London, England, Jan. **1950**, pp. 1–15.

Green, Raymond A., "The Weather and Circulation of February 1966—Strong Blocking Over the Atlantic," *Monthly Weather Review*, Vol. 94, No. 5, May **1966**, pp. 345–350.

Haines, Donald A., and Winston, Jay S., "Monthly Mean Values and Spatial Distribution of Meridional Transport of Sensible Heat," *Monthly Weather Review*, Vol. 91, No. 7, July **1963**, pp. 319–328.

Hastenrath, Stefan L., "The Flux of Atmospheric Water Vapor Over the Caribbean Sea and the Gulf of Mexico," *Journal of Applied Meteorology*, Vol. 5, No. 6, Dec. **1966**, pp. 778–788.

Holopainen, E. O., "On the Role of Mean Meridional Circulations in the Energy Balance of the Atmosphere," *Tellus*, Vol. 17, No. 3, Stockholm, Sweden, Aug. **1965**, pp. 285–294.

Holopainen, E. O., "A Note on the Use of a Forecast as the First Guess in Objective Analysis," *Tellus*, Vol. 20, No. 1, Stockholm, Sweden, Jan. **1968**, pp. 129–131.

Lahey, James F., Bryson, Reid A., Corzine, Harold A., and Hutchins Charles W., "Atlas of 300 Mb Wind Characteristics for the Northern Hemisphere," *Final Report*, Contract No. AF19(604)–2278, University of Wisconsin Press, Madison, **1960**, 1 p. text plus numerous charts.

Lorenz, Edward N., "The Nature and Theory of the General Circulation of the Atmosphere," *World Meteorological Organization Publication* No. 218, Geneva, Switzerland, **1967**, 161 pp.

Oort, Abraham H., "The Observed Annual Cycle in the Meridional Transport of Atmospheric Energy," *Journal of the Atmospheric Sciences*, Vol. 28, No. 3, Apr. **1971***a*, pp. 325–339.

Oort, Abraham H., Geophysical Fluid Dynamics Laboratory, NOAA, Princeton, N.J., Sept. **1971***b* (personal communication).

Palmén, Erik H., "On the Maintenance of Kinetic Energy in the Atmosphere," *The Atmosphere and the Sea in Motion*, The Rockefeller Institute Press, New York, N.Y., **1959**, pp. 212–224.

Palmén, Erik H., and Vuorela, L. A., "On the Mean Meridional Circulations in the Northern Hemisphere During the Winter Season," *Quarterly Journal of the Royal Meteorological Society*, Vol. 89, No. 379, London, England, Jan. **1963**, pp. 131–138.

Peixoto, José P., "Hemispheric Temperature Conditions During the Year 1950," *Scientific Report* No. 4, Contract No. AF19(604)–6108, Planetary Circulations Project, Massachusetts Institute of Technology, Cambridge, Mass., **1960**, 72 pp.

Posey, Julian W., "The Weather and Circulation of January 1966—A Temperature Pattern Reversal Associated With an Index. Cycle," *Monthly Weather Review*, Vol. 94, No. 4, Apr. **1966**, pp 275–282.

Smagorinsky, Joseph, "Some Aspects of the General Circulation," *Quarterly Journal of the Royal Meteorological Society*, Vol. 90, No. 383, London, England, Jan. **1964**, pp. 1–14.

Stark, L. P., "The Weather and Circulation of March 1966—Generally Mild and Dry," *Monthly Weather Review*, Vol. 94, No. 6, June **1966**, pp. 419–425.

Starr, Victor P., and Wallace, J. M., "Mechanics of Eddy Processes in the Tropical Troposphere," *Pure and Applied Geophysics*, Vol. 58, No. 2, Basel, Switzerland, Feb. **1964**, pp. 138–144.

Starr, Victor P., and White, Robert M., "Balance Requirements of the General Circulation," *Geophysical Research Papers* No. 35, U.S. Air Force Cambridge Research Center, Bedford, Mass., Dec. **1954**, 57 pp.

Wiin-Nielsen, A., Brown, John A., and Drake, Margaret, "On Atmospheric Energy Conversions Between the Zonal Flow and the Eddies," *Tellus*, Vol. 15, No. 3, Stockholm, Sweden, Aug. **1963**, pp. 261–279.

Winston, Jay S., "Preliminary Studies of Atmospheric Energy Parameters," *Meteorological Satellite Laboratory Report* No. 3, U.S. Weather Bureau, Washington, D.C., Jan. **1961**, 30 pp.

[Received August 18, 1971; revised April 18, 1972]

The Generation of Available Potential Energy by Infrared Cooling: A Summer Case

T. A. MacKenzie
and
Lyle H. Horn

1. Introduction

Over the past fifteen years a number of investigators has attempted to estimate the various parts of the atmospheric energy cycle. Most of the earlier studies during this period were based on the approximate forms of the available potential energy equations developed by Lorenz (1955a). The results of these investigations have been summarized by Oort (1964). More recently, the equations of Dutton and Johnson (1967), Smith (1969) and Johnson (1970) have been used in estimating the energy cycle. These later equations, which are similar to those obtained by Lorenz (1955b) in a less well-known work, represent the exact form of the energy equations. When studying the generation of available potential energy by diabatic processes it is particularly important that the exact form of the equations be used since these equations give the thermodynamically consistent result that on an isentropic surface heating at high pressure and cooling at low pressure produce a positive generation. In this paper the exact form of the generation equation is used to estimate the generation of available potential energy by infrared radiational cooling during a summer synoptic case.

The exact form of the generation equation has been used by a number of investigators to estimate the generation in limited regions of the atmosphere. Smith and Horn (1969) have applied the equation to a region encompassing most of North America for a one-month period. Using the same data, Hahn and Horn (1969) investigated the evolution of the in situ generation associated with individual cyclones which moved through the region. In both of these studies the thermodynamic method was used to estimate the total heating.

Because of the difficulty in obtaining satisfactory estimates of the total atmospheric heating in limited regions, studies have been conducted which estimate the heating associated with each of the diabatic components. Bullock and Johnson (1971) examined the contribution of the release of latent heat to the available potential energy of a spring storm over the central United States. The importance of the generation of available potential energy by sensible heating has been studied by Gall and Johnson (1971) for a late winter North Atlantic cyclone and by Bullock and Johnson (1972) for cyclones over the Southern ocean. Min and Horn (1973) have investigated, in a climatological sense, the generation by sensible heating in the cyclogenetic regions along the east coast of Asia and North America. The results of all of the above-mentioned studies indicate that latent and sensible heating play significant roles in the generation of available potential energy.

The importance of infrared cooling in the generation is less well-established. Most of the infrared studies have employed the approximate form of the generation equation. Suomi and Shen (1963) used infrared radiation measurements made from the Explorer VII satellite and 1000 to 100 mb thickness maps to estimate the generation in a mid-latitude region. They found that the mean generation was slightly positive with large daily fluctuations. Corcoran and Horn (1965) computed the covariance of the outgoing long-wave radiation measurements made by Tiros II and the 1000 to 500 mb thickness field to estimate the generation associated with various 500 mb wave patterns. They concluded that the shorter wavelength patterns, with their relatively systematic cloud distributions, are sites of a small positive generation of available potential energy due to infrared cooling, while the generation associated with the longer wave patterns is slightly negative. Johnson (1967) also used the Lorenz approximation to estimate the infrared component of the generation. Using data from radiometersonde flights made over the eastern United States and the Caribbean, he arrived at generation values which were negative when temporally averaged, but varied greatly from day to day. Bullock and Johnson (1971) were the first to use the exact form of the generation term to estimate the effect of infrared cooling in a mid-latitude cyclone. Assuming a uniform cooling rate of $-1.4\,^{\circ}C$/day, they obtained positive generation values ranging up to $+1.19$ watts/m^2. Using cooling rates of -1.0 and $-1.8\,^{\circ}C$/day for the cloudy and clear regions, respectively, values of the generation reached a maximum of $+2.25$ watts/m^2. Anthes and Johnson (1968) have estimated that the generation by infrared cooling in hurricane Hilda amounted to $+0.6$ watts/m^2 for a 1000 km radius area.

The intent of this study is to use the exact form of the generation equation to examine in more detail the role of differential infrared cooling in the generation of available potential energy in a limited region of North America for a June, 1966, situation. Models of the vertical distribution

of infrared cooling and Nimbus II radiation data were employed. Within the area chosen for this study there was an extratropical cyclone over the northcentral United States and a tropical cyclone (Hurricane Alma) near the Florida Gulf coast. The generation was calculated for the whole area and also separately for the extratropical cyclone.

2. The Basic Equations

The time rate of change of available potential energy for any volume is defined by Johnson (1970) to be

$$\frac{dA}{dt} = G(A) - C(A, K) + B(A) + W(A) \tag{1}$$

where $G(A)$ is the generation of available potential energy, $C(A, K)$ is the conversion of available potential energy to kinetic energy within the volume, $B(A)$ is the advection through the boundary, and $W(A)$ is the pressure work done on the boundary.

This study is concerned with the in situ generation of available potential energy, which in pressure coordinates is

$$G(A) = \frac{1}{g} \int_{\sigma} \int_{p} [1 - (\frac{p_r}{p})^{\kappa}] Q_m \, dp d\sigma \tag{2}$$

where Q_m is the rate of diabatic heating, p is the atmospheric pressure of a point in the volume, p_r is the mean or reference pressure of the isentropic surface which passes through that point, g is gravity, and σ is the horizontal area of the region considered. This equation is the same as the expression obtained by Smith (1969). The quantity

$$\varepsilon = [1 - (\frac{p_r}{p})^{\kappa}] \tag{3}$$

usually referred to as the efficiency factor, is a measure of the effectiveness of heating or cooling in changing the available potential energy of the region being considered. If heat is added at pressures higher than the reference pressure of an isentropic surface or extracted at pressures lower than the reference pressure, $G(A)$ is positive and available potential energy is generated.

Since the vertical integration is done in pressure coordinates, the rate of heat loss is expressed as the divergence of the net radiation in a column between two pressure surfaces. Assuming that the horizontal divergence of radiation is negligible for a narrow column that is horizontally stratified, the rate of cooling can be expressed in finite difference form as

$$Q_m = g \frac{\Delta F_n}{\Delta p} \tag{4}$$

where ΔF_n is the difference of the net radiation between the top and bottom of the vertical column defined by Δp. For further discussion, see Smith et al. (1965). In finite difference form, the mean generation of available potential energy can then be expressed as

$$G(A) = \frac{1}{\sigma} \sum_{\sigma} \sum_{p} \varepsilon \, \Delta F_n \Delta\sigma \tag{5}$$

if the increment of pressure used to obtain the divergence of the radiation is the same as that used in the vertical summation.

3. The Synoptic Case

In this study the infrared component of the generation was estimated for the time period near 1630Z 9 June 1966. It was necessary to confine the study to this time because it was the only time that adequate Nimbus II medium resolution infrared radiation data used to determine the infrared cooling were available. On the afternoon of 9 June, an active extratropical cyclone was moving through Indiana as a stable wave bringing rain to much of the Great Lakes region. At the same time, Hurricane Alma was moving northward along the Gulf coast of Florida. The Nimbus II advanced vidicon camera system (AVCS) composite photograph in Figure 1 shows the distribution of the clouds associated with these two storms at approximately 1630Z 9 June. At this time the clouds associated with each vortex appear as separate systems, although the cloud systems did merge on the following day. The 500 mb maps of Figure 2a and b are for 12Z 9 June and 00Z 10 June. The features most important to this study are the closed low of the hurricane near Florida and the short-wave moving across the western Great Lakes in association with the open wave cyclone at the surface. The surface maps of Figure 3a and b show the hurricane approaching the Florida coast and an open wave cyclone moving from northcentral Illinois at 15Z into northern Indiana at 18Z 9 June.

Figure 4, a nephanalysis of the hourly surface observations made at 16Z 9 June is divided into three panels depicting the low, middle and high clouds based on the standard synoptic code height categories. To aid interpretation of the charts, a fifth category has also been added. In the middle and high cloud panels, the regions bounded by scalloped lines indicate where higher clouds may be present, but lower clouds make verification from the ground impossible. In using the conventional and satellite data, a rectangular grid similar to the National Meteorological Center (NMC) grid but with twice the grid point density was employed for the

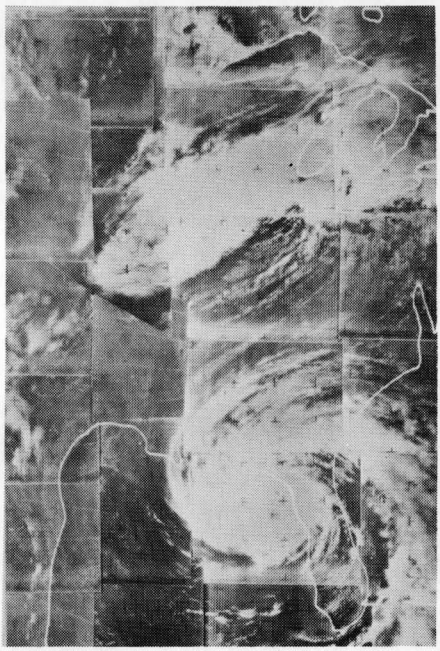

Figure 1. Nimbus II AVCS composite photograph for 1630Z June 9, 1966.

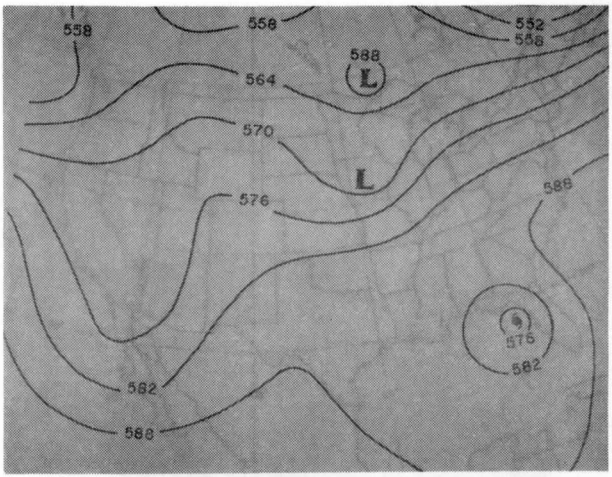

Figure 2a. The 500 mb constant pressure analysis of geopotential height for 1200Z 9 June 1966.

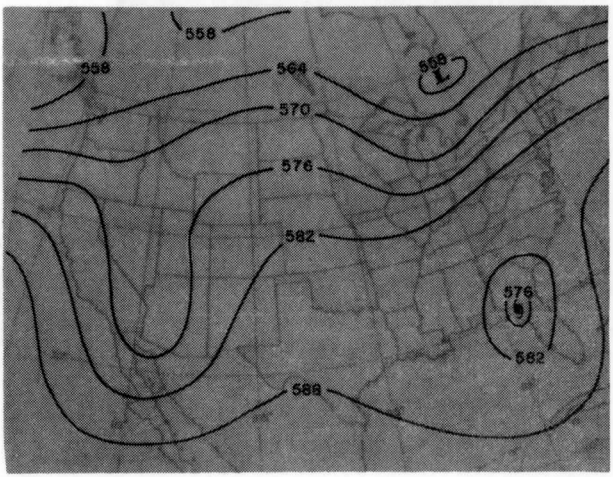

Figure 2b. Same as Figure 2a but for 0000Z 10 June 1966.

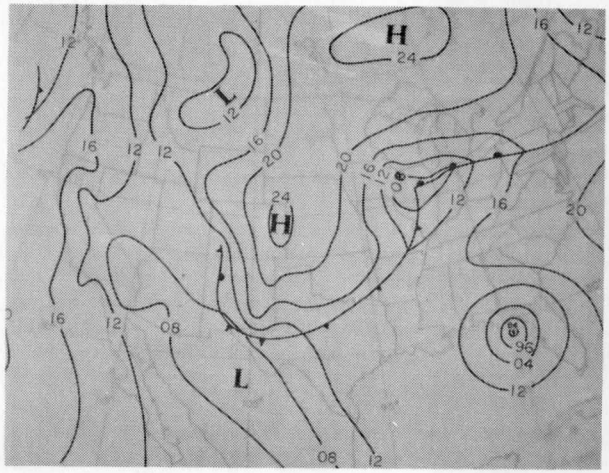

Figure 3a. NMC surface analysis for 1500Z 9 June 1966.

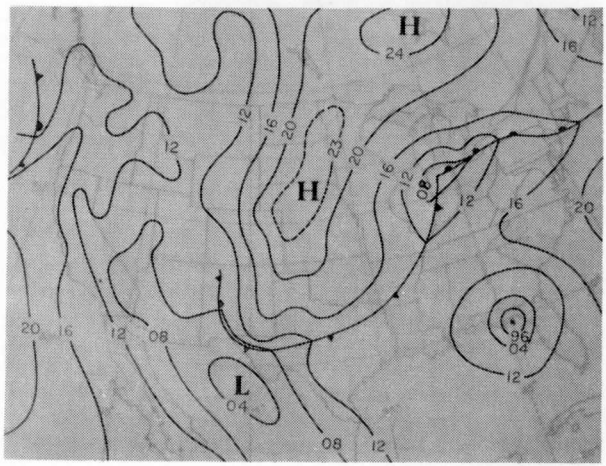

Figure 3b. Same as Figure 3a for 1800Z 9 June 1966.

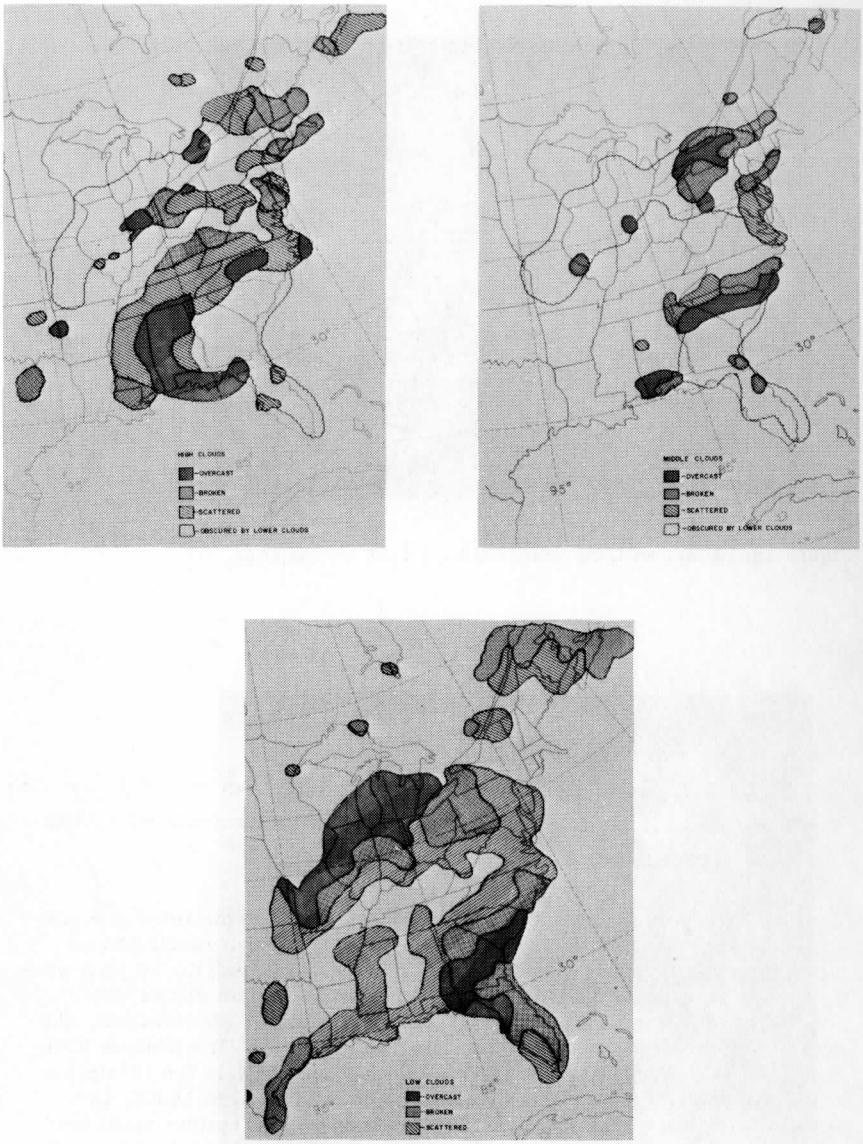

Figure 4. Nephanalysis of surface hourly observations made at 1600Z 9 June 1966.

various analyses used in the study. Upper air data for 12Z 9 June and 00Z 10 June were interpolated to this grid which is shown in Figure 5.

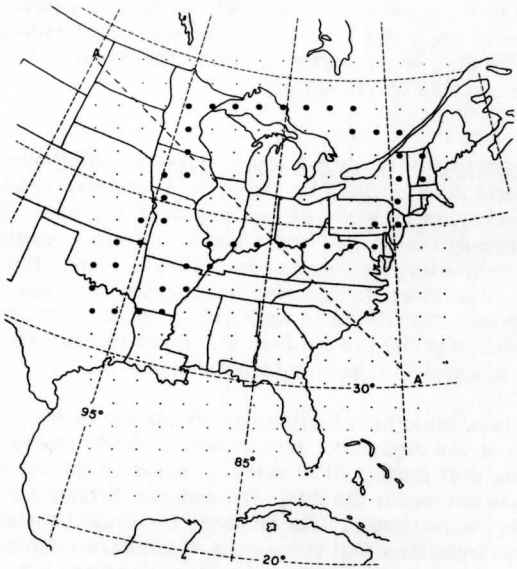

Figure 5. Small dots: grid of Nimbus II data and to which 12Z 9 June 1966 and 00Z 10 June 1966 sounding data were interpolated. Large dots: boundary points of small area.

a. The potential temperature distribution—Since the reference pressure used to define the efficiency factor in Eq. (4) is for isentropic coordinates, the upper air sounding data for 12Z 9 June and 00Z 10 June were converted to isentropic coordinates. Fourteen isentropic charts from 285°K to 350°K were then analyzed for the 12Z and 00Z observations, the data being interpolated to the grid shown in Figure 5. (The Nimbus II infrared radiation data were interpolated to the same grid.) The isentropic data for these two times were then linearly interpolated to 1630Z, the approximate time of the satellite observations. Since neither storm was intensifying nor weakening rapidly during this time period, the assumption of linearity of the pressure and temperature data is quite reasonable for a volume of this size.

The pressure distribution representative of low, middle and high isentropic surfaces is shown in Figures 6, 7 and 8, respectively. The low isentropic surface (295°K) intersects the ground along the dashed line in Figure 6. For computational purposes, the distribution of pressure on the portion of an isentropic surface which is below the surface of the earth is assumed to be the same as the pressure at the earth's surface. All three isentropic surfaces show the baroclinic zone (region of strongest gradient of pressure) to lie across the northern United States with the coldest air in the northeastern section of the region.

b. The distribution of efficiency factor—The reference pressure on an isentropic surface as defined by Dutton and Johnson (1967) is simply the area weighted mean pressure of the isentropic surface. The reference pressures for each of the 14 isentropic surfaces were computed and plotted as a function of potential temperature in Figure 9. Since the vertical cooling distribution is most easily handled in pressure coordinates, the potential temperature was calculated at each grid point at 50 mb intervals. The reference pressure was then taken from the graph in Figure 9, and the efficiency factor computed for each grid point using Eq. (3).

Since in isentropic coordinates the efficiency factor is a single-valued function of the pressure, the isentropic charts in Figures 6, 7 and 8 also depict the distribution of efficiency factor on the isentropic surfaces. The reference pressures for the 295, 310 and 325°K isentropes are 922, 657 and 426 mb, respectively. On all three isentropic surfaces the pressure distribution indicates that the region of positive efficiency factors is larger than the region of negative efficiency factors, but the gradient of pressure (and therefore efficiency factor) is much greater to the north of the zero efficiency factor line than it is to the south. If the volume were to include more of the cold air north of the extratropical cyclone, the zero efficiency factor line would be shifted farther into the colder air. The choice of the boundaries of the region can play an important role in determining the efficiency factor distribution and thus generation of available potential energy.

A diagonal cross-section of the potential temperature and efficiency factor distributions is shown in Figure 10. The zero efficiency factor line has the S-shaped curve noted by Hahn and Horn (1969), Gall and Johnson (1971), and Bullock and Johnson (1971), with a sign change also taking place near the tropopause in both the positive and negative areas. In both the positive and the negative regions the largest absolute values of efficiency factors are in the upper regions of the troposphere, but the absolute values of efficiency factor are greater in the negative region than they are in the positive region.

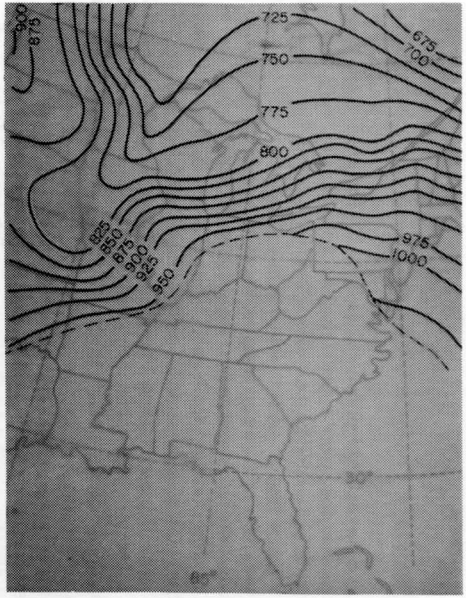

Figure 6. Pressure distribution (mb) on the 295° K isentropic surface for 1630Z 9 June 1966.

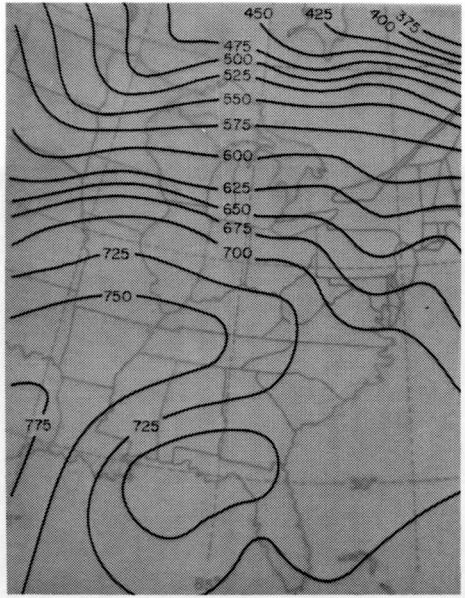

Figure 7. Same as Figure 6 for the 310° K isentropic surface.

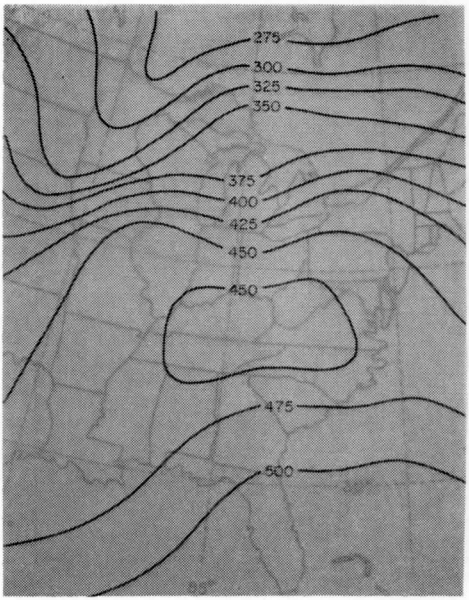

Figure 8. Same as Figure 6 for the 325°K isentropic surface.

4. The Cooling Models

The generation of available potential energy by infrared cooling requires the existence of a covariance between the cooling and efficiency factors. Although it is more difficult to describe the distribution of infrared cooling within a large region of the atmosphere than it is the efficiency factor field, balloon-borne radiometersonde observations combined with satellite observations can be employed to model the cooling. In this paper three models of the cooling are used. Two are based on relatively simple statistical correlations of radiometersonde data and satellite infrared measurements. The third is based on a semi-subjective synthesis of various statistical information derived from radiometersonde observations. Variations of the third are also used to test what effect raising or lowering the cloud top height estimate has on the generation of available potential energy by infrared processes. Finally, as a test of the influence of the configuration of the efficiency factor field on the generation, the uniform cooling rate of -1.4 °C/day, used by Bullock and Johnson (1971), was also applied to this study.

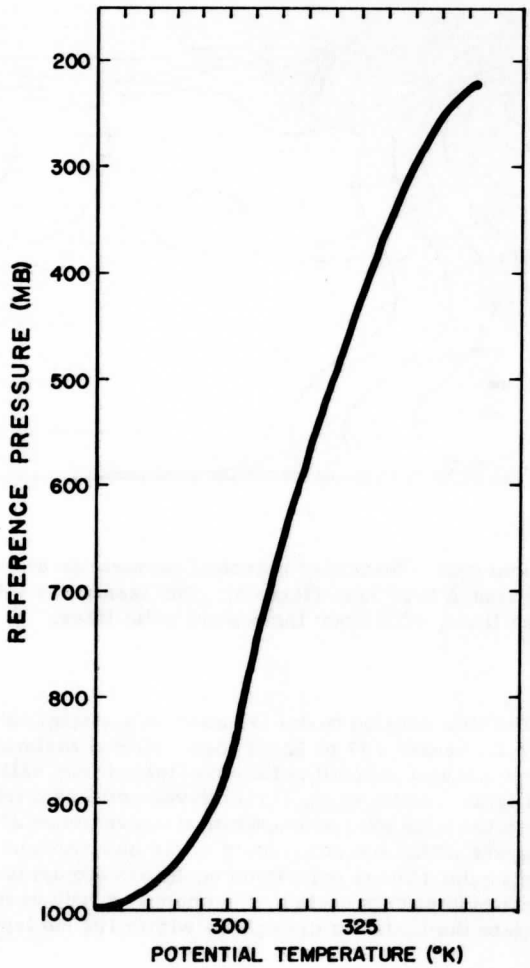

Figure 9. Reference pressure as a function of potential temperature.

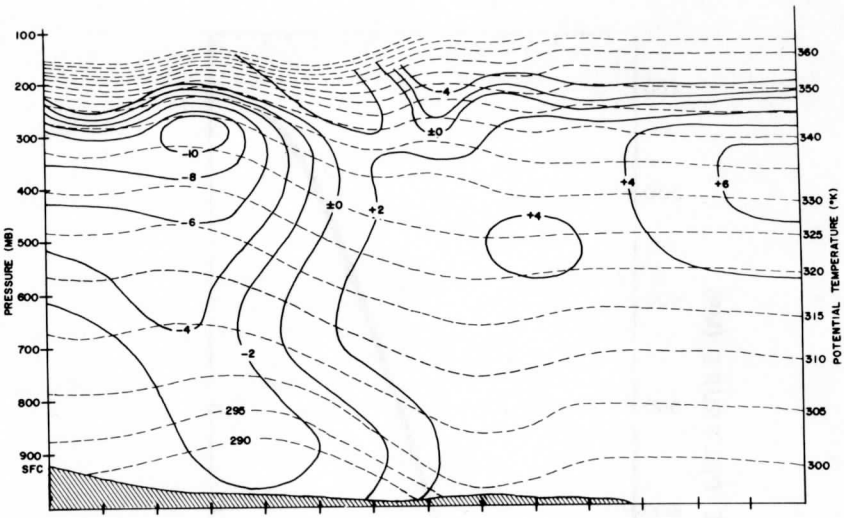

Figure 10. Diagonal cross-section of potential temperature and efficiency factor from A to A' (see Figure 5). The isentropes (°K) are the dashed lines, efficiency factors are solid lines.

Model 1. The first cooling model is based on a statistical correlation between Tiros II channel 4 (7 to 32 microns) infrared radiation measurements and the divergence of infrared radiation obtained from balloon-borne radiometersonde flights. Smith et al. (1966) developed linear regression equations (listed in the appendix) which relate the divergence of net radiation for various layers within the atmosphere to the observations made by the satellite. For Model 1 these regression equations are applied to the upward irradiance measurements made by the channel 4 radiometer aboard Nimbus II to estimate the radiative divergence within 100 mb layers beneath the satellite.

Model 2. The second cooling model is also based on the correlations between Tiros II observations and the divergence of infrared radiation obtained by Smith et al. (1966), but with the data divided into two groups: those for observations of clear or scattered sky conditions, and those for which the observations showed broken or overcast clouds.

Model 3. The third cooling model was based on the careful analysis of 113 balloon-borne radiometersonde flights which reached to at least the 50 mb level. At levels higher than 50 mb the radiometersonde measurements of the upwelling infrared radiation should approach those measured by a satellite-based instrument. The divergence of radiation (and thus cooling) within each 100 mb layer was calculated from the radiometersonde data and expressed as a percentage of the outgoing radiation measured at the top of the sounding. The Nimbus II observations were then treated as if they were observations made at the top of the balloon flight, and the cooling in each 100 mb layer estimated using the percentages obtained from the model.

In developing the model the radiometersonde data were smoothed by passing a five-point smoother through the vertical array of data points for each sounding. Since the model was to be used to distribute the cooling in an independent data sample (i. e., the Nimbus II data), the smoothing was done to reduce the rather large variability which exists in the vertical in individual radiometersonde observations. The smoothed data were divided into classes based on cloud conditions at the time of the observation. Average profiles of cooling were computed for conditions of clear, low cloud tops and high cloud tops.* These averages, supplemented by the mean cooling rates derived by Cox (1969) and the infrared cooling described by Johnson (1967) and Johnson and Shen (1968), were then used to subjectively obtain various models of the vertical distribution of infrared cooling. The final models provided cooling profiles for clear, low cloud top and high cloud top conditions, with the cooling in the 100 mb layer expressed in terms of a percentage of the outgoing radiation measured at the top of the sounding (or by the satellite). The clear cases were divided into clear-dry or clear-moist, the division being arbitrarily made at a surface dew point temperature of 55°F. The groups of low and high cloud tops were divided, depending on whether the observation shows broken or overcast clouds at the specified grid point. In some cases thin overcast conditions were treated as broken because of the lower emissivity of thin clouds. Figures 11, 12 and 13 illustrate the cooling profiles obtained from the model.

In both of the clear case models, the greatest cooling is in the lowest layers of the atmosphere. In the moist case, however, the cooling is displaced somewhat upward due to the radiative properties of the moist layer. Thus, in Figure 11 the moist case shows slightly less cooling in the layer below 900 mb, but more cooling between 900 and 700 mb. Above the moist layer the two curves coincide since the cooling is relatively independent of the moisture near the surface.

*The 675 mb level was used to separate low and high cloud tops.

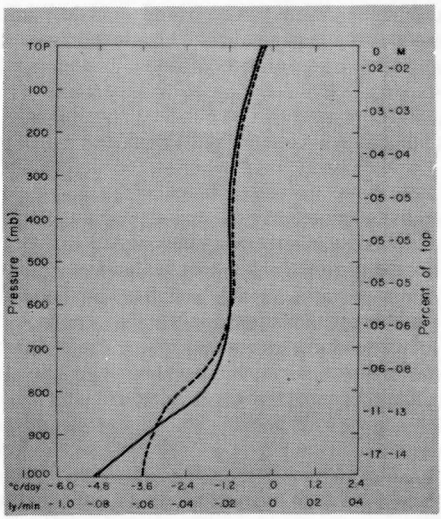

Figure 11. Model 3 for clear skies, with an example of cooling profiles obtained for a satellite channel 4 flux measurement of 0.40 ly/min. Solid line for "dry" (D) surface observation (T_d < 55°F), dashed line for "moist" (M) surface observation ($T_d \geq 55°F$). Numerical values of divergence per 100 mb in terms of a percent of the satellite measurement are shown to the right.

The low cloud top version of Model 3 (Figure 12) shows strong cooling in the 100 mb layer immediately above the clouds, with the cooling decreasing rapidly upward from the cloud tops. Within the clouds, approximate radiative equilibrium should exist. In the rather limited layer below the low cloud deck, there is little or no cooling because the clouds form a radiative cap for the atmosphere below. For broken rather than overcast conditions, the effective emissivity, which Smith (1967) defines as the product of the emissivity of the clouds and the number of tenths of cover, is decreased. Thus with broken clouds, less cooling is shown in the region above the clouds and more cooling beneath the clouds. The region more than 200 mb above the clouds probably cools relatively

independently of the variations in cloud amount, so the two cooling profiles shown in Figure 12 coincide at heights well above the cloud deck.

The model for high cloud tops shown in Figure 13 is similar to the low cloud profiles in the region above the clouds, but in the region near the base of the clouds slight warming is indicated. The slight warming was based on the premise that usually the temperature at the base of these higher clouds will be colder than the earth's surface and lower regions of the atmosphere, and thus will be warmed by radiative processes. As in the case of the low cloud tops, different cooling profiles were used for broken and overcast cases.

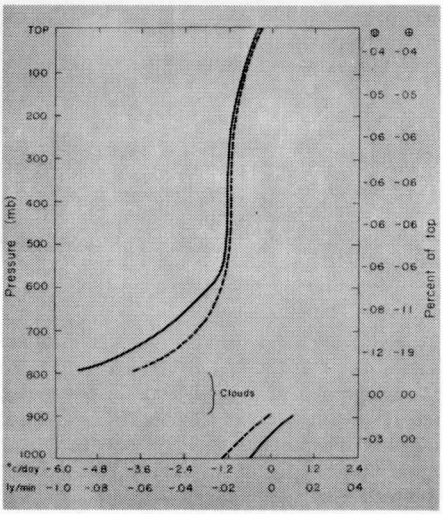

Figure 12. Model 3 for low clouds (tops at 700 mb or lower) with an example of a cooling profile obtained for a satellite channel 4 flux measurement of 0.35 ly/min. The solid line represents the cooling distribution for overcast clouds, and the dashed line the cooling distribution for broken sky conditions. In this example the cloud top was placed at 800 mb and the base at 900 mb. Numerical values of divergence per 100 mb in terms of a percent of the satellite measurement are shown to the right.

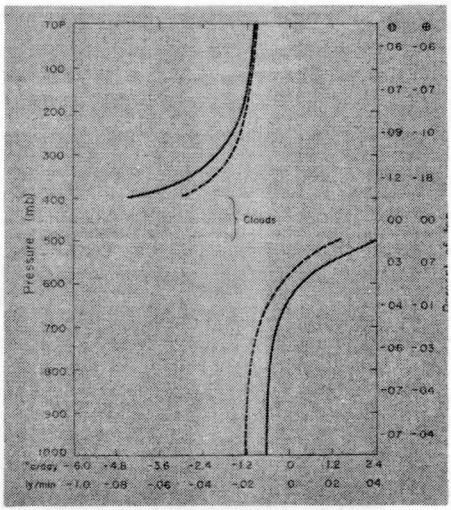

Figure 13. Model 3 for high clouds (tops at 650 mb or higher) with an example of a cooling profile obtained for a satellite channel 4 flux measure of 0.28 ly/min. The solid line represents the cooling distribution used with overcast clouds, and the dashed line represents the cooling distribution for broken sky conditions. In this example the cloud tops were placed at 400 mb and the base at 500 mb. Numerical values of divergence per 100 mb in terms of a percent of the satellite measurement are shown to the right.

Examples of the performance of the three models for a high cloud top case and a clear case are shown in Figure 14. The observed cooling profile in panel A was obtained from a balloon-borne radiometersonde flight over Montgomery, Alabama in a cirrus overcast situation. In this case, Model 3 is clearly superior; however, this accuracy may be somewhat deceptive. In the general application of the model the determination of the level of cloud tops and bottoms is often less accurate than it is in this example. A further examination of Figure 14(A) reveals that Models 1 and 2 provide reasonable estimates of the cooling immediately above the cloud tops, but because they are of a statistical nature the cloud top cooling is arbitrarily placed at the mean cloud top height of the statistical sample.

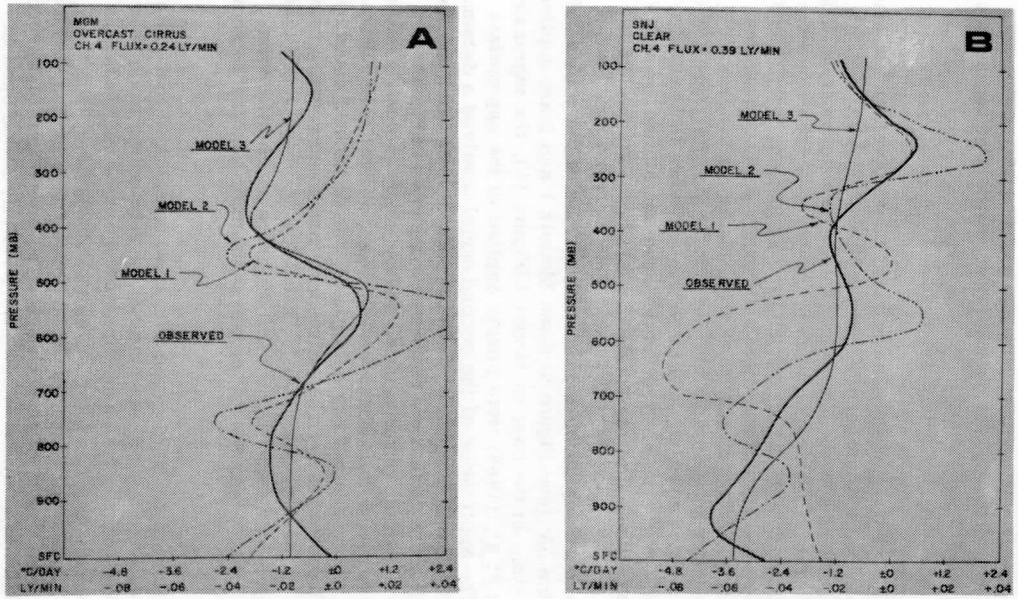

Figure 14. The vertical distribution of the cooling predicted by each of the three models compared to the cooling distribution observed by balloon-borne radiometersonde flights at (A) Montgomery, Alabama, 6 January 1961, and (B) San Juan, Puerto Rico, 23 December 1960.

Figure 14(B), based on a radiometersonde flight over San Juan, provides a comparison of the responses of the models for a clear, moist condition. Model 3 provides a good estimate of the cooling below 400 mb but misses the slight warming between 200 and 300 mb. Although Model 1 responds to this high level warming, it greatly overemphasizes the middle and high level variations in the cooling.

a. Application of the models—The infrared cooling values used in this study were obtained using channel 2 and 4 Nimbus II data and the cooling models described above. The Nimbus data were taken from NASA medium resolution grid. On this grid each point value is representative of the radiation measurements made over an area equivalent to 1/30 of the area represented by one grid point on the NMC grid. Radiation values were then read off the NASA grid and transferred to the grid shown in Figure 5, which is twice as dense as the NMC grid. An analysis of the channel 4 total outgoing radiation data in ly/min is shown in Figure 15. The regions of high cloud tops associated with the two storms are indicated by the areas of low outgoing radiation.

Figures 16 and 17 depict vertical cross-sections of the cooling obtained along the line AA' (see Figure 5) when Models 1 and 2 are applied to the Nimbus II data. In the case of Model 1 (Figure 16), the regression equations of Smith et al. (1966) were simply applied to the appropriate channel 4 data. The application of the second model involved a determination of the cloud distribution within the area represented by each grid point. This was accomplished by using the nephanalysis shown in Figure 4, which was based on surface observations, and by using channel 2 and 4 satellite data where the surface observations were not available. In regions of high broken or overcast sky conditions, the channel 2 equivalent black-body radiative temperatures are quite low, and the channel 4 total outgoing radiation values are also small. The AVCS photograph of Figure 1 also aided in the determination of cloud conditions at each grid point. The cooling distribution along the AA' cross-section for Model 2 is shown in Figure 17.

The application of the third model was more complex in that it was necessary to decide which of the six versions of the cooling model should be used at each grid point. The estimation of the height and thickness of the clouds involved the combined use of the nephanalysis of Figure 4, the channels 2 and 4 Nimbus data, the AVCS composite photograph (Figure 1), and the 12Z 9 June 1966 radiosonde data. The equivalent black-body radiative temperature data from channel 2 were heavily relied upon in determining the level of cloud tops except when other information such as radiosonde data or hourly observations implied broken or thin overcast cloud layers. For example, in regions where the nephanalysis indicated high overcast conditions, but the channel 2 black-body temperatures were

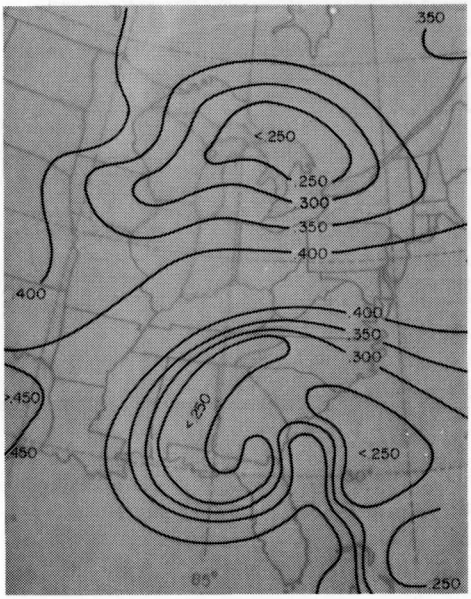

Figure 15. Channel 4 infrared radiation (ly/min) measured by the radiometer aboard Nimbus II on 9 June 1966.

relatively high, it was assumed that the overcast was thin and therefore had a low emissivity. In such cases the overcast was treated as broken, and thus as having a lower effective emissivity. The cooling field along the AA' cross-section obtained using Model 3 is presented in Figure 18.

A comparison of the distribution of the cooling obtained from the three models can be made by examining the three cross-sections shown in Figures 16, 17 and 18. The linear regression equations of Model 1 place the maximum cooling in the layer between 600 and 700 mb in response to the mean cloud top height for the total data sample used by Smith et al. (1966). The strongest cooling at these levels, however, is in the clear regions rather than the cloudy regions because of the large channel 4 measurement obtained in clear regions. Application of the second cooling model corrects this somewhat by shifting the maximum cooling into the cloudy regions, but the strong cooling is still concen-

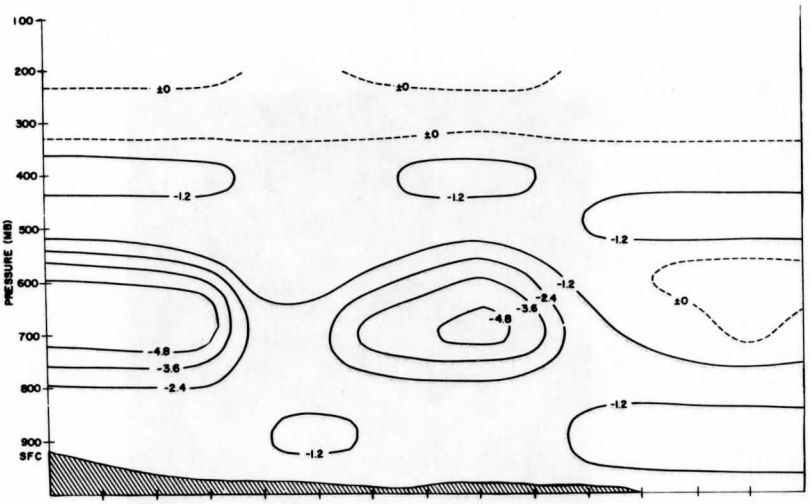

Figure 16. Cross-section from A to A' (see Figure 5) of the cooling distribution for Model 1 (°C/day).

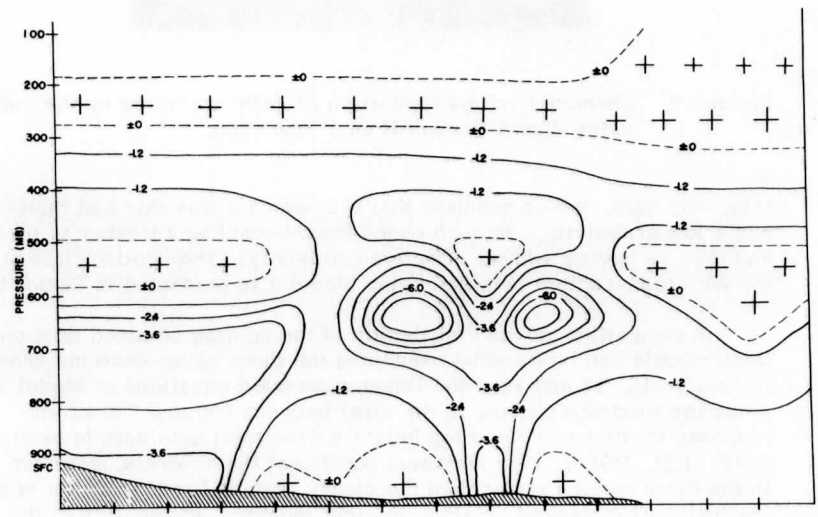

Figure 17. Same as Figure 16 for Model 2.

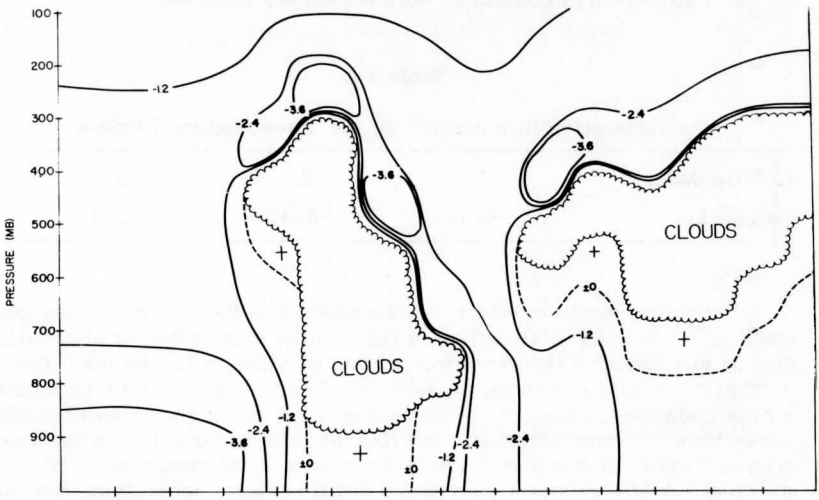

Figure 18. Same as Figure 16 for Model 3.

trated in the 600 to 700 mb layer regardless of the cloud top height. The decrease of cooling under the clouds and the increase in the cooling near the surface in the clear regions is also more realistically accomplished by the second model. Within the regions of thin overcast, though, the second model responds too strongly because of the relatively large channel 4 values. In these cases the cooling should be more evenly distributed throughout the depth of the atmosphere. The third model yields the most realistic distribution of the cooling. The maximum cooling is immediately above the clouds, rather than tied to a mean cloud top height, and the amount of cooling in the layers just above and just below the clouds is more realistically related to the effective emissivity of the clouds.

5. The Generation

The cooling fields obtained from the models described in the previous section and the efficiency factor field described earlier were combined to estimate the generation of available potential energy due to infrared cooling within the budget area shown in Figure 5. The estimates obtained from the three models, which are listed in Table 1, are all small negative numbers; however, there is a tendency for the generation to become

more positive (i. e., less negative) in going from Model 1 (the crudest model) to Model 3, indicating that the generation estimates become larger as the distribution of cooling is more accurately modeled.

Table 1

The Generation in watts/m^2 for the Three Cooling Models

Cooling Model	1	2	3
Generation	-0. 52	-0. 44	-0. 13

To further test the effect of the modeling of the cooling on the generation, the vertical distribution of the cooling was varied by arbitrarily raising and lowering the cloud top heights of Model 3 by 100 mb. The generation results are shown in Table 2. Lowering the cloud tops produces a more negative generation, while raising them produces a small positive generation. Raising the cloud tops has the effect of displacing the maximum cooling to higher levels where the efficiency factors tend to be more negative. While this test produced a small positive generation, the value of +0. 06 watts/m^2 cannot be considered significant to the energy budget of the volume.

Table 2

The Generation in watts/m^2 for Model 3 for Three Different Estimates of the Cloud Top Heights

Model 3	down 100 mb	original	up 100 mb
Generation	-0. 26	-0. 13	+0. 06

An inspection of Eq. (3) reveals that the mean efficiency factor on an isentropic surface is negative since pressures lower than the reference pressure yield larger absolute values of the efficiency factor than do the same size deviations on the higher side. Thus a simple uniform cooling field should generate available potential energy. Bullock and Johnson (1971), using a uniform infrared cooling rate of -1. 4°C/day for a budget volume containing a major March cyclone, obtained generation estimates of +0. 85, +1. 19 and +1. 13 watts/m^2 for the cyclogenetic, mature and occluded stages. To further test the effect of uniform cooling the -1. 4°C/day value was applied to the budget volume for this summer case. A

generation of +0.24 watts/m^2 was obtained. The smaller, although positive, value obtained here is likely due to the weaker baroclinity which exists in June. The absolute magnitudes of the efficiency factors are greater for more steeply sloping isentropic surfaces.

Since a uniform cooling rate produced a positive generation, the negative estimates presented in Table 1 must result from a substantial negative covariance between the cooling and efficiency factors in portions of the budget volumes. In order to obtain a better understanding of which portions of the volume were mainly responsible for the destruction, the generation values at the 850 and 250 mb levels were analyzed. The results are presented in Figures 19 and 20. In general, the areas north of the zero efficiency factor lines ($\varepsilon = 0$) are areas in which cooling produces a positive generation while to the south cooling destroys available potential energy. However, there are some anomalous regions where infrared warming occurred such as at the base of the high cloud layers. In the cloudy regions at 850 mb (see Figure 19) the generation is zero since radiative equilibrium exists within the clouds. At 850 mb the absolute magnitude of the positive and negative generations are comparable, but the geographical region over which negative generation occurred is larger. The destruction resulting from the infrared cooling of the clear tropical air is especially apparent from eastern Texas northeastward into the Ohio valley. The mean contribution of the 850 mb level was -1.23 watts/m^2. At 250 mb the absolute values of the positive and negative generation values are comparable, but at this higher level the region containing positive generations is larger than at 850 mb. Thus the 250 mb level contributed an areal mean of +0.22 watts/m^2.

The choice of a volume is often critical in determining whether the generation estimates for a particular diabatic process are positive or negative. For example, Hahn and Horn (1969) have shown that if the entire atmosphere is used to obtain the efficiency factor field, the regions of positive and negative efficiencies may be quite different from those obtained for a more limited region. Because the volume used in this study contained both an extratropical and a tropical cyclone, it was decided to separately compute the efficiency factor field for the region containing the extratropical cyclone and obtain generation estimates for this smaller volume. The smaller region is indicated by the large points in Figure 5. The clear region separating the clouds of the tropical cyclone from those of the extratropical cyclone was used to position the southern boundary of the smaller volume (See Figure 1). Only the Model 3 cooling estimates were used for the smaller volume. For this smaller volume a mean generation estimate of -1.2 watts/m^2 was obtained. Although the zero efficiency factor line was shifted northward when the smaller volume was used, the strong cooling from the clear warm air just south of the extratropical cyclone was sufficient to produce a mean negative generation. Figures 21 and 22, similar to 19 and 20,

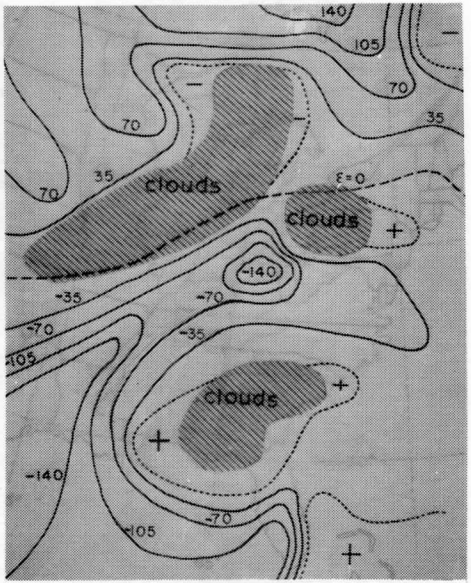

Figure 19. The mean contribution from the 850 mb level is -1.23 watts/m^2 (solid lines). Dotted lines are anomalous region discussed in the text; dashed line is the zero efficiency factor line.

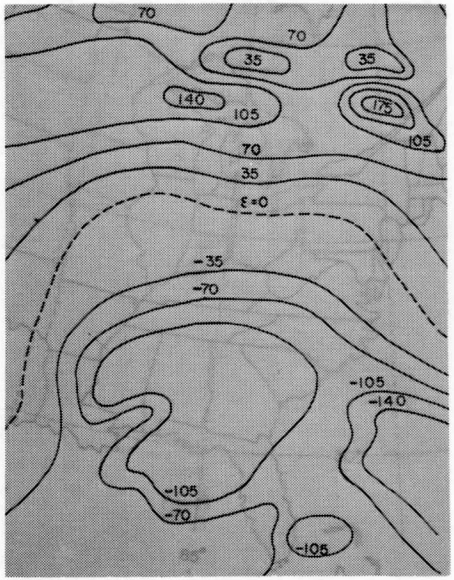

Figure 20. Same as Figure 19 for the 250 mb constant pressure surface. The mean contribution from the 250 mb level is +0.22 watts/m^2.

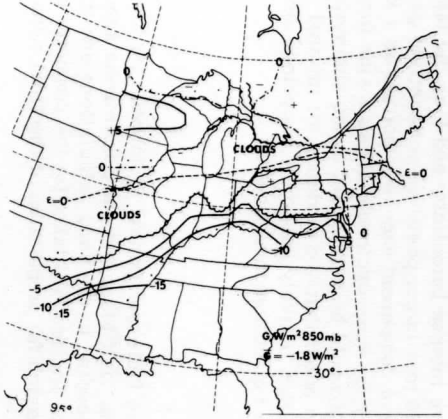

Figure 21. Same as Figure 19 for the small volume. Mean generation is -1.8 watts/m^2.

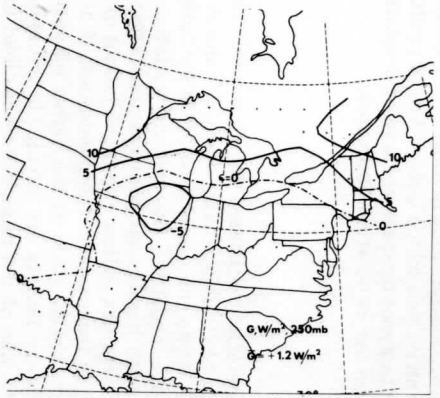

Figure 22. Same as Figure 21 for the small volume. Mean generation is 1.2 watts/m^2.

show the contributions from the 850 and 250 mb levels. Again the low level cooling leads to a negative contribution (-1.8 watts/m^2 at 850 mb). At 250 mb the mean contribution to the generation is positive (+1.2 watts/m^2). Thus in this synoptic case the use of a smaller volume has no appreciable effect on the generation estimates.

6. Conclusions

Although the generation estimates due to infrared cooling for the case studied here were negligibly small, certain features of the generation should be noted. While the mean generation for both the large and small volumes is slightly negative, the vertical variation of the generation is considerable, with significant positive generation occurring at high elevation. These results indicate that the height of the clouds, especially their tops, is important to the generation of available potential energy at the storm scale. It is at the higher elevations that the largest negative efficiency factors are found. In the applications of the three models and in the use of the three different cloud top estimates for Model 3, the generation estimates increased as the cloud tops were raised.

The results obtained here indicate that, while the generation by infrared cooling was insignificant for this volume, it is likely to be significantly positive for some synoptic situations and negative for others, with the particular cloud distribution being the controlling factor. In winter cases the more intense baroclinity and thus the larger efficiency factors may well lead to a larger positive (or negative) generation. Thus the role of the infrared component may be important as a source of available potential energy for some cyclones and as a sink for others. Such a variability in itself would be significant in the energetics of cyclones. Finally, it should be noted that the tendency for infrared cooling to aid in static destabilization is likely important in cyclone development and should be the subject of further investigation.

Acknowledgments

Thanks are due Professor Donald R. Johnson for his frequent discussions of the problem. Jeff Maer and Larry Scheinoha should be thanked for the many days devoted to the hand calculations and the authors are also indebted to Mr. Thomas Whittaker for the computer programming and to Sandra Markevich for preparation of the final manuscript.

The drafting of the figures was well executed by Mike Lin and Dan

Dolson, and the assembly and photograph of the Nimbus II mosaic was done by Dave Cadle of the University of Wisconsin Space Science and Engineering Center.

References

Anthes, R. A. and D. R. Johnson, 1968: Generation of available potential energy in hurricane Hilda (1964), MWR, Vol. 96, No. 5, pp. 291-305.

Bullock, B. R. and D. R. Johnson, 1971: The generation of available potential energy by latent heat release in a mid-latitude cyclone, MWR, Vol. 99, No. 1.

_____, 1972: The generation of available potential energy by sensible heating in Southern Ocean cyclones, Quart. Jour. of the Roy. Met. Soc., Vol. 98, No. 417, pp. 459-518.

Corcoran, J. L. and L. H. Horn, 1965: The role of synoptic scale variations of infrared radiation in the generation of available potential energy, J. Geoph. Res., Vol. 70, No. 18.

Cox, S., 1969: Radiation models of mid-latitude synoptic features, MWR, Vol. 97, No. 9.

Dutton, J. A. and D. R. Johnson, 1967: The theory of available potential energy and a variational approach to atmospheric energetics, Adv. in Geoph., Vol. 12.

Gall, R. L. and D. R. Johnson, 1971: The generation of available potential energy by sensible heating: A case study, Tellus, Vol. 23, pp. 466-482.

Hahn, D. and L. H. Horn, 1969: The generation of available potential energy in a mid-latitude cyclone, Final Rept., ESSA Grant WBG 52, Dept. of Meteorology, University of Wisconsin, Madison.

Johnson, D. R., 1967: The role of terrestrial radiation in the generation of zonal and eddy available potential energy, Tellus, Vol. 19, No. 4, pp. 517-539.

_____, 1970: The available potential energy of storms, J. Atmos. Sci., Vol. 27.

_____ and W. C. Shen, 1968: Profiles of infrared irradiance and cooling through a jet stream, MWR, Vol. 96, No. 8.

Lorenz, E. N., 1955a: Available potential energy and the maintenance of the general circulation, Tellus, Vol. 7.

_____, 1955b: Generation of available potential energy and the intensity of the general circulation, Final Rept., Large Scale Synoptic Processes, Dept. of Meteorology, University of California, Los Angeles, J. Bjerknes, Project Director.

Min, K. D. and L. H. Horn, 1973: The generation of available potential energy by sensible heating along the east coasts of Asia and North America, Submitted for publication to the Journal of the Meteorological Society of Japan.

Oort, A. H., 1964: On estimates of the atmospheric energy cycle, MWR, Vol. 92, No. 11.

Petterssen, S., D. L. Bradbury, and K. Pedersen, 1962: The Norwegian cyclone models in relation to heat and cold sources, Geophys. Publik., Vol. 24, No. 9.

Smith, P. J., 1969: On the contribution of a limited region to the global energy budget, Tellus, Vol. 21.

_____ and L. H. Horn, 1969: A computational study of the energetics of a limited region of the atmosphere, Tellus, Vol. 21, No. 2, pp. 193-201.

Smith, W. L., L. H. Horn, and D. R. Johnson, 1966: On the relation between Tiros radiative measurements and atmospheric infrared cooling, J. App. Met., Vol. 5, No. 4.

Smith, W. L., 1967: An iterative method for deducing tropospheric temperature and moisture profiles from satellite radiation measurements, MWR, Vol. 95, No. 6.

Suomi, V. E. and W. C. Shen, 1963: Horizontal variations of infrared cooling and the generation of eddy available potential energy, J. Atmos. Sci., Vol. 20, No. 1.

Appendix. Linear regression coefficients of Smith, Horn and Johnson (1965) relating the upward flux of radiation measured by the Tiros II channel 4 radiometer (F_s) to the net divergence of the radiation flux (ΔF_n) in 100 mb layers for Models 1 and 2. ($\Delta F_n = b_1(F_n) + b_0$) b_1 is nondimensional, b_0 in ly/min.

	Model 1		Model 2			
			clear and scattered		broken and overcast	
pressure (mb)	b_1	b_0	b_1	b_0	b_1	b_0
100-200	.1508	-.0487	.1695	-.0569	.2031	-.0606
200-300	.0050	-.0045	-.0591	.0018	-.0311	.0011
300-400	.0893	-.0134	.0753	-.0110	.1472	-.0272
400-500	-.1307	.0592	-.0196	.0235	-.1843	.0761
500-600	.4936	-.1385	.0240	-.0145	.6684	-.1979
600-700	.5381	-.1321	.1837	-.0344	1.0941	-.2742
700-800	.0855	.0040	.3409	-.0787	-.0220	.0392
800-900	.1545	-.0283	.2041	-.0397	.0208	.0043
900-Sfc	.0418	.0136	.2021	-.0212	-.4194	.1267

An Application of the Satellite Indirect Sounding Technique in Describing the Hyperbaroclinic Zone of a Jet Streak

by

William E. Togstad* and Lyle H. Horn
University of Wisconsin

ABSTRACT

Often important weather producing features such as the jet streak are not adequately resolved at the input stage of numerical models. The satellite indirect sounding technique offers promise of greatly increasing observational detail. An 18 March 1971 case study is used to test the ability of the SIRS algorithm to resolve the thermal support of a jet streak. Isentropic cross sections through the streak are prepared and 17 synthetic soundings are obtained. The sounding data are reduced to equivalent irradiances, and the SIRS algorithm is used to retrieve the thermal structure for various assumed observational errors, grid spacings, and initial guess profiles. While an observational error of 0.25 ergs $(cm^2\text{-sec-sr } cm^{-1})^{-1}$ permits the reconstruction of the general wind field, accuracies to within 0.10 and preferably 0.05 ergs are required to resolve the essential structure of the jet streak's thermal support.

1. Introduction

The recent success in inferring the thermal structure of the atmosphere from satellite-measured irradiances promises to provide the meteorologist with a vast increase in upper air data. Accompanied by an appropriate refinement in the numerical models, the increase in input data should subsequently lead to improved weather prediction. Smith et al. (1970) have shown that in some cases the combination of the experimental SIRS (Satellite Infrared Spectrometer) data with conventional radiosonde data can improve the accuracy of medium range numerical prognostic charts over those based on the radiosonde data alone. It is

*Present affiliation: Meteorological Satellite Laboratory, National Environmental Satellite Service, Washington, D. C.

noteworthy that the cases of improved numerical predictions were accomplished using the SIRS instrument which is not only experimental but also has a relatively low resolution.

In the near future a number of additional satellites containing various sounders capable of retrieving soundings with both improved spatial resolution and orbital coverage will be operational. The first of these, Nimbus 5, containing an infrared (ITPR) and a microwave (NEMS) sounder, was launched in December 1972. Eventually observations provided by sounders such as these should improve the numerical prediction products by: 1) providing a global or near-global grid, thus reducing boundary problems; 2) providing good input data for areas which now have poor conventional data coverage; and 3) providing a much finer retrieval of data, thus revealing the existence of smaller scale features which presently are often lost at the input stage. With regard to point 3, it is well recognized that an accurate forecast of the long wave pattern is often not sufficient for an accurate forecast of the weather. The scale of many precipitation-producing disturbances is frequently much smaller than the scale of the long wave features in which they are imbedded. Because of the large gaps between conventional radiosonde stations, especially outside the continental United States, the input data for numerical forecasts fail to reveal these small scale features. Furthermore, the small scale disturbances propagate more rapidly than the long wave features. Thus the 12 hour time interval between radiosonde observations is sometimes too great to maintain sufficient continuity.

The propagating jet streak is an important small scale feature which may be missed in the objective analysis of upper air data. Since the timing and positioning of cyclogenesis and severe weather outbreaks are dependent on the position of the jet streak, its inclusion in the input data for numerical models is essential to weather prediction. In this paper are reported the results of a case study designed to test the ability of the SIRS sounding retrieval technique to locate and describe the thermal support of a jet streak.

2. The Nature and Importance of Jet Streaks

Numerous observations have demonstrated that the close relationship between the jet stream and the baroclinity associated with the polar front can be used to trace the position of the jet stream around the hemisphere. Along the axis of the jet stream are observed isotach maxima which propagate downwind. Palmen and Newton (1969), who have labelled these maxima jet streaks, have discussed the dimensions of individual streaks in relation to the wind strength within the streak. Newton (1954) has shown that jet streaks are found over the most intense portions of the hyperbaroclinic zone, while the lower wind speed areas including the leading and trailing parts of the jet streak (i.e. the delta and entrance zones, respectively) are associated with broader, weaker zones of

baroclinity. This is, of course, consistent with the thermal wind relationship.

Because the speed of propagation of most streaks is typically between 20 and 40 knots while the actual wind speeds are often over 100 knots, air parcels passing through the streaks will first experience a positive and then negative acceleration. The acceleration of transient air within the streak is accomplished by cross contour flow. Murray and Daniels (1953) have noted that organized patterns of cross contour flow in jet streaks represented direct and indirect transverse circulations. Rieter (1963) has shown that the transverse circulations produce changes in both the mass distribution and baroclinity which are entirely consistent with the streak's downwind propagation. A great number of investigators have taken note of the importance of the transverse circulations associated with jet streaks in producing vertical motion and in contributing to cyclogenesis and outbreaks of severe weather. See, for example, Riehl (1952), Starrett (1949), Yeh (1950), Johnson and Daniels (1953), Palmen and Newton (1969), and Miller (1967).

Recently, Cahir (1971) has observed that, although numerical prediction has improved the 12-36 hour forecasts, there has not been a comparable improvement in the 0-12 hour forecasts which are often dependent on small scale features such as the propagating jet streak. Obviously, the prediction of such features is not possible unless they can be accurately resolved in the initial analysis. Since the typical width of a jet streak is a few hundred kilometers, the circular searching technique used in the objective analysis often fails to resolve this feature. Even in the data-rich area of the United States, the spacing of radiosonde stations is often too great to provide an adequate resolution. In the data-sparse areas of the Pacific and Atlantic Oceans, the problem becomes exceedingly difficult. However, the indirect sounding technique promises to alleviate these observational difficulties.

3. The Indirect Sounding Technique

The basis of the indirect sounding technique involves the measurement of the infrared radiation leaving the atmosphere in several spectral intervals. Assuming the distribution of absorbing gases is known, radiation arising from a spectral interval near the center of an absorption band is emitted from high altitudes of the atmosphere, while that emitted from the wings of the band is emitted from lower elevations. By the appropriate selection of the spectral intervals and the use of Planck's law, it is possible to interpret the measured irradiances in terms of the atmospheric temperature at various elevations.

The SIRS instruments flown aboard Nimbus 3 and 4 have been described by Wark and Hilleary (1969, 1971), Hanel and Conrath (1969)

and Hanel et al. (1971). The retrievalof a sounding from SIRS observations is accomplished through the iterative procedure described by Smith, Woolf and Fleming (1972). The differences between the radiances associated with an initial guess profile and the satellite observed values are calculated. The iterative procedure attempts to reduce these differences to the point where they fall below the noise level of the instrument. The retrieval sounding is the one which in the convergence alters the guess sounding the least. Because there is nearly complete absorption of upwelling infrared radiation by clouds, it is not possible for the SIRS retrieval technique to obtain the portion of the sounding beneath the clouds. Since the SIRS instrument has a field of view of 225 km, the observations are often contaminated by clouds. Smith, Woolf and Jacob (1970) have described methods of correcting for the presence of partial cloudiness in the field of view. However, the major alleviation of the cloud problem will be accomplished through the use of higher resolution infrared and microwave instruments. For example, as mentioned earlier, Nimbus 5 has aboard an infrared instrument possessing a 60 km resolution and also a microwave instrument capable of obtaining observations from the region beneath a solid cloud deck.

It should also be noted that the SIRS sounding technique falls short in that it does not provide some of the details of the atmosphere's vertical thermal structures. For example, temperature inversions such as those associated with the sloping hyperbaroclinic zone beneath a polar jet, are poorly resolved. This limitation, however, is not as severe as it may first appear, since the lack of vertical detail is compensated for by excellent horizontal detail. The synoptic meteorologist is accustomed to extracting much information concerning the horizontal characteristics of the thermal field from the rich data sample obtained along the vertical axis of a single conventional radiosonde observation. Conversely, it is possible to use the rich array of data in the horizontal provided by numerous indirect soundings to reconstruct the detailed vertical structure. It is noteworthy that future satellites will have polar orbits which improve the horizontal spacing of soundings over those made by the SIRS instruments. More importantly, future geosynchronous satellites, such as the proposed ATS-G and SMS-B, will be capable of sensing the earth's disc at frequent intervals, thus providing the opportunity to sound in great detail those regions of the atmosphere which are meteorologically active on a given day. Finally, it should be noted that the inclusion of a 4.3μm CO_2 band sensor may significantly improve the vertical resolution of features such as frontal inversions. See Smith (1972) for a discussion of the improvement obtained when a 4.3μm band is included.

4. The General Procedure

To test the ability of the SIRS sounding technique to resolve the thermal support of a jet streak, a case study involving a late winter storm

was undertaken. Using the conventional radiosonde network, isentropic cross sections were carefully constructed to describe the detailed thermal structure of the atmosphere in the area of the suspected jet streak. Although features as small as the jet streak are difficult to locate using the conventional upper level charts, they can often be located through the careful but time-consuming analysis of isentropic cross sections. Cahir (1971) and Duquet et al. (1964), for example, emphasize that isentropic cross sectional analysis of conventional radiosonde data achieves the best possible resolution of subsynoptic features.

From the isentropic cross sections synthetic soundings were extracted at 1° latitude (111 km) intervals. Those soundings and the thermal wind relationship were used to calculate the isotachs of the wind component normal to the cross section. This analysis was then used as a standard with which a similar analysis based on the retrieved soundings (described below) could be compared.

The synthetic sounding data extracted from the cross section were converted to equivalent irradiances, which were then treated as if they were observations made by the SIRS instrument. The SIRS algorithm (see Smith, Woolf and Jacob, 1970) was then applied to the observations in an attempt to retrieve the original synthetic soundings. In the processing of the irradiances the retrieval procedure was programmed to introduce various degrees of observational error. This was done in order to assess the effect of the various levels of error on the ability of the procedure to retrieve sounding data of sufficient quality to resolve the thermal support of the jet streak.

5. The Synoptic Case and the Sounding Retrieval Procedure

Since it is often difficult to determine whether a well-developed jet streak is present in a given synoptic situation, careful attention was given to selection of a case for study. The synoptic case of 12Z 18 March 1971, was chosen as appropriate. Figures 1-3 portray the surface, 500 mb and 300 mb analyses of the situation.

Thirty-six hours before the time period chosen for the case study, a 500 mb ridge was situated off the west coast of North America with a broad trough downstream. A short wave imbedded in the northwest flow east of the ridge was present in southwestern Canada. As the short wave amplified and propagated southeastward, a surface low developed over northern Nevada. The surface low deepened and moved eastward spreading snow north of its center as it crossed the Great Basin and moved into the Rockies. The most rapid intensification of the surface low occurred as it moved off the mountains of Colorado. By 12Z of the 18th, an intense storm was positioned on the Kansas-Nebraska border (see Figure 1). North and west of the storm center a very tight pressure gradient existed

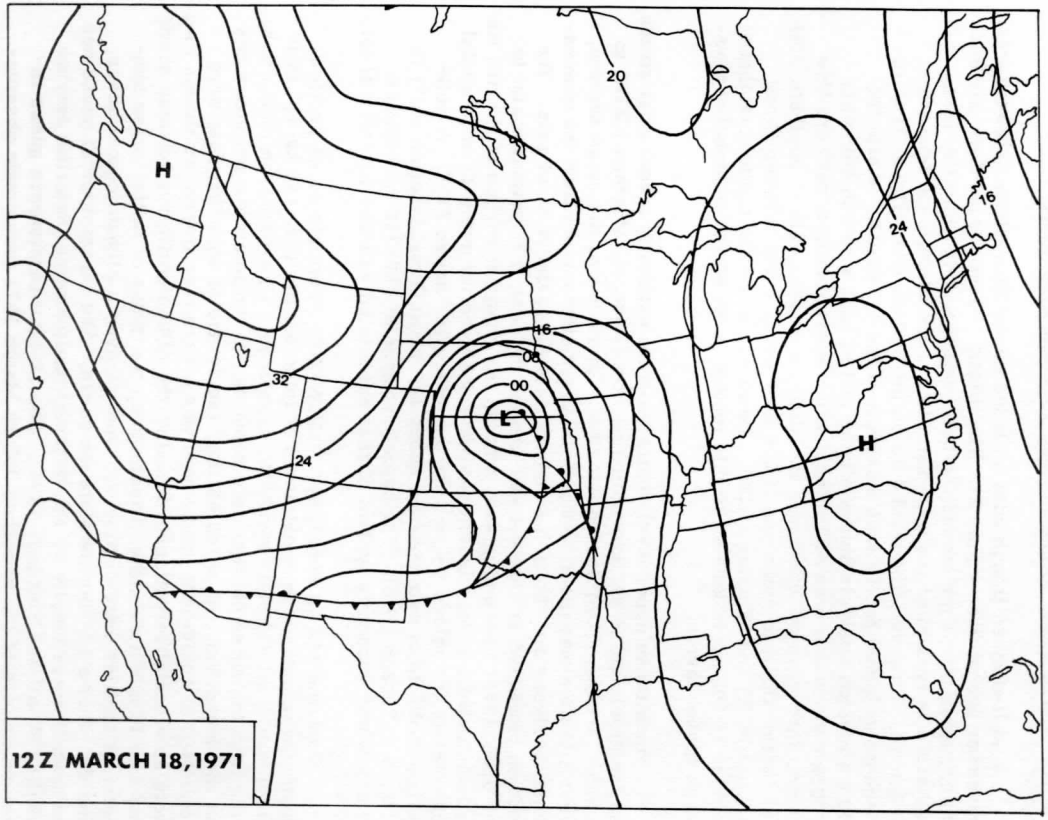

Figure 1. Surface analysis for 12Z March 18, 1971

with blizzard conditions. Many areas reported near zero visibility with winds between 50 and 60 mph and gusts to 80 mph. Southeast of the storm severe thunderstorms and a few tornadoes were reported in the lower Mississippi Valley. A heavy snow shield spread northeast of the storm into portions of Iowa, Minnesota and southern Wisconsin.

A well-defined trough with a closed center in western Nebraska was present at 500 mb (see Figure 2). The strong 500 mb temperature gradient which curves from Utah around the bottom of the trough into the Texas panhandle is typical of the hyperbaroclinic zone often found beneath a jet streak. However, the wind data on the 300 mb chart(Figure 3) is inadequate to locate the isotach maximum of the jet streak. While the 300 mb isotach analysis shows a band of 100 knot winds in Idaho and Oregon and another area of 100 knot winds extending from northern New Mexico into western Oklahoma, the absence of wind data in southern Utah makes it difficult to determine if 100 knot winds exist between Grand Junction (GJT) and Winslow (INW). However, since the tightest isotherm packing at 500 mb is located in this region, a jet streak is probably present at higher levels.

Since these upper level charts failed to explicitly reveal a jet streak, the isentropic cross section extending from Glasgow, Montana (GGW) to Tucson, Arizona (TUS) was constructed. In analyzing the cross section, great attention was given to maintaining consistency between the conventional analyses and the rich supply of data along the vertical axis. The section presented in Figure 4 was chosen because it is perpendicular to the upper level flow and passes through the sharpest portion of the 500 mb hyperbaroclinic zone. Isentropes were analyzed for every 2° of potential temperature for values below 373K and every 10° above 373K. A well-defined polar front extends from about 425 mb at Grand Junction (GJT) to 925 mb at Tucson (TUS). The baroclinic zone at 250-350 mb between Winslow and Tucson is typical of that associated with the subtropical jet.

From the 12Z 18 March 1971, GGW-TUS isentropic cross section synthetic soundings were extracted at intervals of every 111 km (1° latitude) giving a total of 17 synthetic soundings. Using Poisson's equation, data from the cross section were converted to temperatures and pressures for the soundings. As noted earlier, the synthetic sounding data were converted to equivalent irradiances which were then treated as though they were satellite observations. In using the SIRS algorithm to retrieve sounding data from the simulated irradiances, two types of initial guess temperature profiles were employed. One involved a climatological guess, and the other a 12-hour persistence guess. The climatological guess has been used operationally by the National Environmental Satellite Service (Smith, Woolf and Fleming, 1972). The 12-hour persistence guess involved the use of the smoothed 00Z 18 March 1971 radiosonde observations taken at the five stations in the cross section.

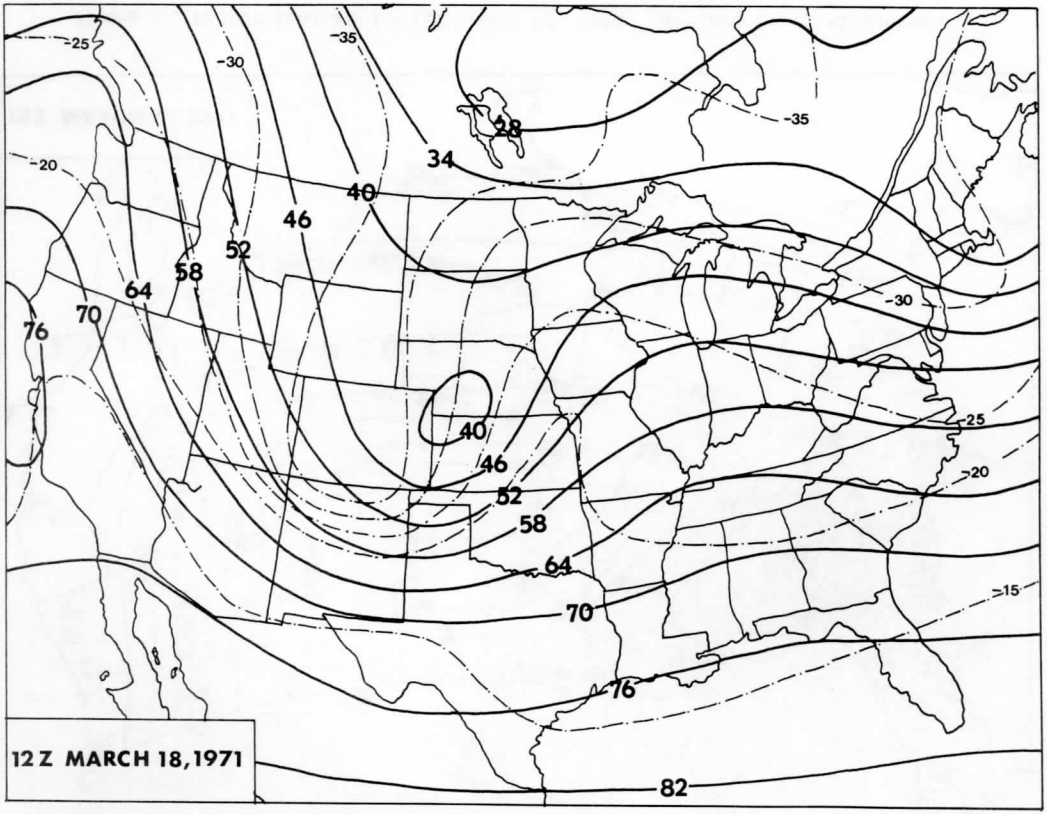

Figure 2. 500 mb analysis for 12Z March 18, 1971. Isotherms at 5°C intervals and contours for every 60 geopotential meters.

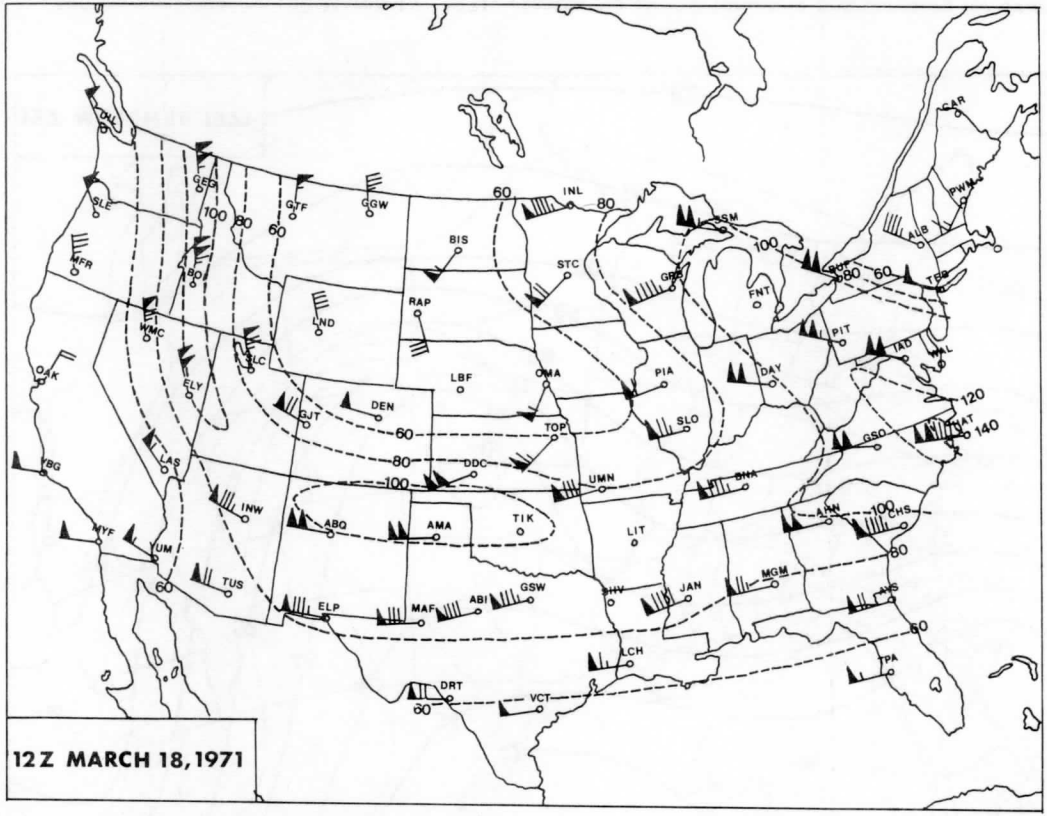

Figure 3. 300 mb analysis for 12Z March 18, 1971. Isotachs for 20 kt intervals.

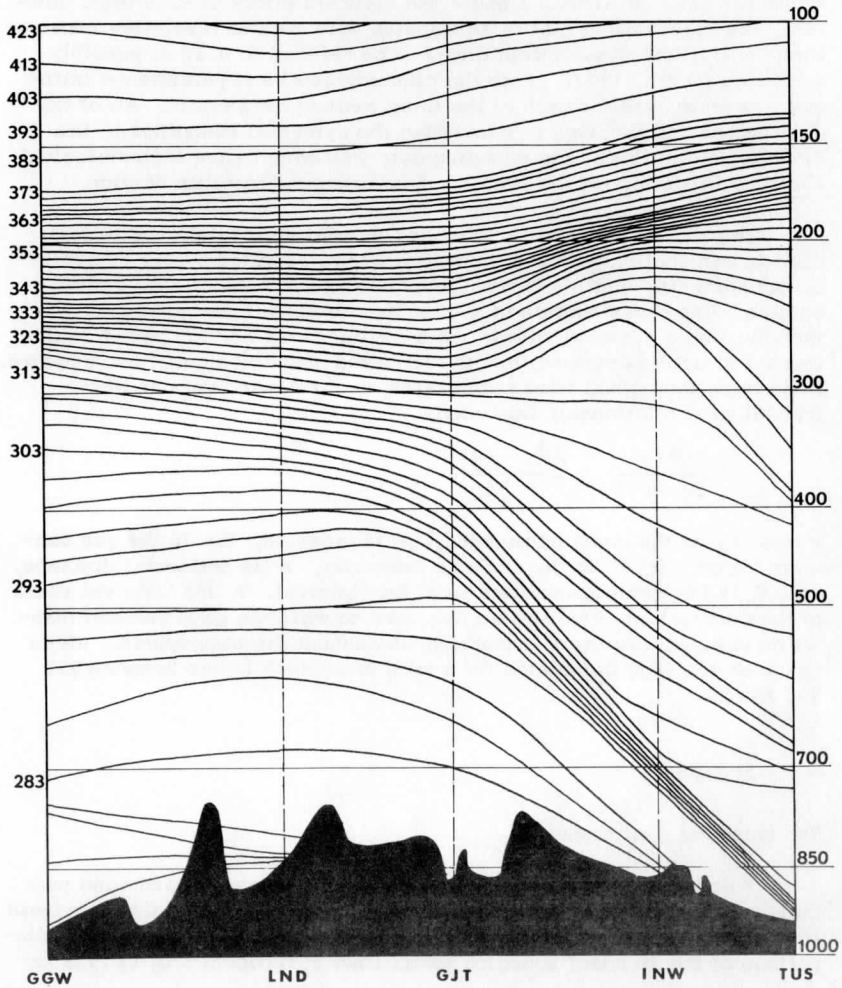

Figure 4. Isentropic cross section from Glasgow, Montana to Tucson, Arizona for 12Z March 18, 1971. Isentropes at intervals of 2°C below 373°K and 10°C intervals above 373°K.

In order to assess the effect of measurement error on the quality of the retrieved soundings, each retrieval program was run for an assumed error of 0.25, 0.10, and 0.05 ergs $(cm^2\text{-sec-sr } cm^{-1})^{-1}$*. The SIRS instruments used on Nimbus 3 and 4 had standard errors of 0.25 ergs; however, the improvement that is anticipated with medium resolution instruments will allow measurement errors to be reduced to 0.10 or possibly 0.05 ergs (Smith, 1972). Both the climatological and persistence initial guesses were used for each of the three measurement errors. All of the data processing involved in converting the synthetic soundings to irradiances and retrieving the sounding data was done by the Meteorological Satellite Laboratory of the National Environmental Satellite Service.

The 700 mb geostrophic wind and thermal wind relationship were used in conjunction with the thermal structure supplied by the 17 synthetic soundings to obtain a derived wind component normal to the cross section. The cross section of the isotachs obtained in this manner was then used as a standard with which a similar cross section based on the thermal structure obtained from the retrieved soundings could be compared. In deriving the normal wind components, the following version of the thermal wind relationship was used:

$$\frac{\Delta V_g}{\Delta(-\ell n\ p)} = -\frac{R_d}{f}\left(\frac{\Delta \bar{T}}{\Delta n}\right)$$

where V_g is the geostrophic wind, p is pressure, R_d is the gas constant for dry air, f is the Coriolis parameter, n is horizontal distance, and $\bar{T}$ is the mean temperature in a ℓnp interval. A ℓnp interval equal to the constant ℓn 950/850 mb was used to maintain good vertical resolution (i.e. a minimum of smoothing) throughout the troposphere. Mean temperatures were calculated for a total of 20 such layers between 950 and 100 mb.

6. Results

The Retrieval Soundings

Before comparing the retrieved fields of temperature and wind with their standards, it may be instructive to compare two individual retrieved soundings with the original synthetic sounding. Figure 5 provides a comparison of the standard sounding (solid line) at retrieval site 13 (333 km

---

*Hereafter in this paper the assumed errors will be simply referred to as 0.25, 0.10 or 0.05 ergs without including the complete but cumbersome units.

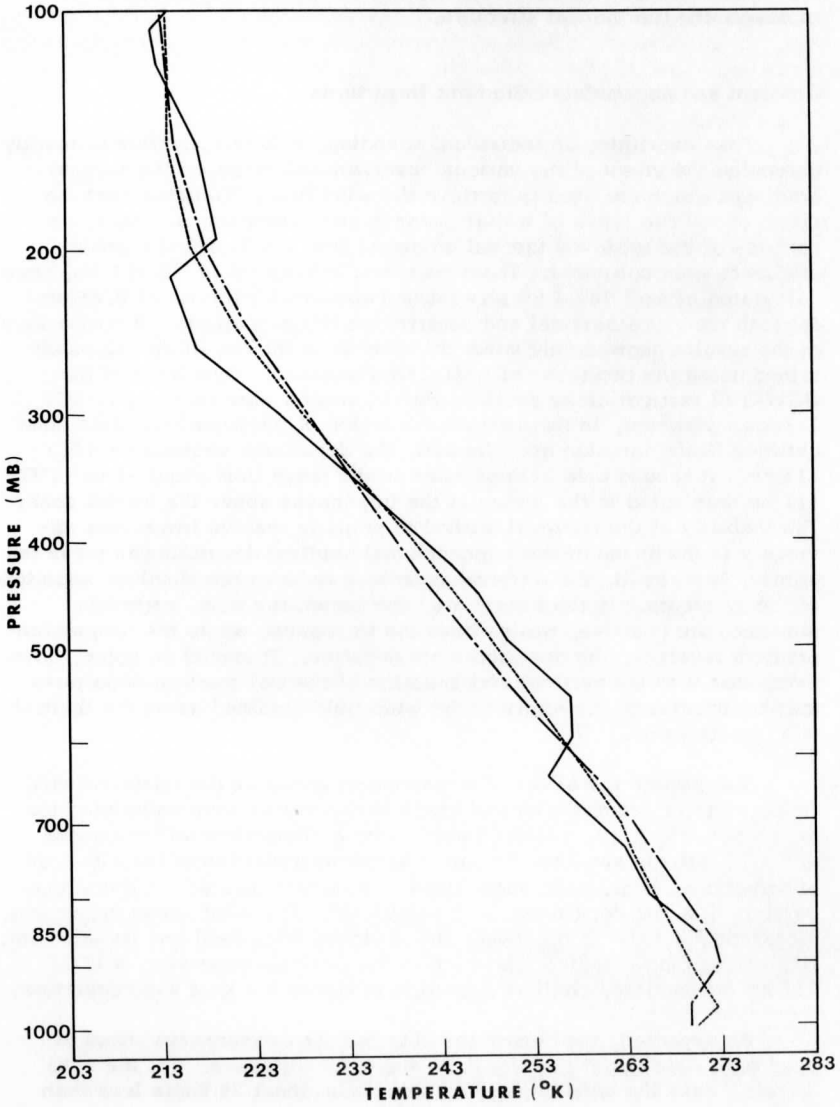

Figure 5. Synthetic sounding number 13 from GGW-TUS cross section (solid line) and its simulated retrievals with assumed observational errors of 0.25 ergs (dash-dotted line) and 0.05 ergs (dashed line).

south of GJT), with retrieval soundings (dashed lines) obtained from observations assumed to possess errors of 0.05 and 0.25 ergs, respectively. In both cases only the general temperature profile is retrieved; the frontal inversion and tropopause are poorly resolved. It is apparent, however, that the sounding retrieved assuming a 0.05 error is substantially better in describing the thermal structure.

Gradient and Accumulated Gradient Departures

From examining an individual sounding, it is not possible to readily determine the effect of the various observational errors on the thermal gradients which are used to retrieve the wind field. To better test the effect of the two types of initial guesses and observational errors, departures of the retrieved thermal gradients from the standard thermal gradients were computed. The departures, expressed in °C/111 km, were calculated at each level for an assumed observational error of 0.25 ergs for both the climatological and persistence initial guesses. A comparison of the results showed only minor differences in the departure values obtained using the two types of initial first guesses. Over most of the GGW-TUS vertical cross section, the departures were within $\pm$ 1.5°C/111 km. However, in the 850-500 mb region of the hyperbaroclinic zone between Grand Junction and Winslow, the departures exceeded + 4°C/111 km. A second area of departures in the range from about -2 to -4°C/111 km was noted in the region of the tropopause above the frontal zone. The inability of the retrieval method to properly resolve inversions obviously is the cause of the larger thermal gradient departures in these regions. As a result, the retrieval technique reduces the absolute magnitude of the gradients. In the frontal area the departures (i.e. retrieval-standard) are positive, while above the tropopause where the temperature gradient reverses, the departures are negative. It should be noted, however, that it is the vertical accumulation of thermal gradient departures that contributes to the errors in the wind field obtained using the thermal wind relationship.

To examine the effect of measurement errors on the retrieved wind field, vertical accumulations of gradient departures were calculated for errors of 0.25, 0.10, and 0.05 ergs using a climatological first guess and a 1° latitude spacing. To gain a better appreciation of the effect of observational error, wind speed departures rather than accumulated temperature gradient departures were calculated. The wind speed departures represent the difference between the retrieved wind field and its standard. Neglecting the latitudinal variation in the Coriolis parameter, a 1°C/111 km accumulated gradient departure produces a 6 knot wind departure.

As expected, the departures obtained for measurement errors of 0.25 ergs were larger than for 0.10 and 0.05 erg errors. For the 0.25 erg error case the wind departures range from about 75 knots less than

their standard just above the frontal zone to about 50 knots greater than the standard above the tropopause in the same region. Thus above the frontal zone the wind field is greatly smoothed. A similar pattern of smoothing occurred for measurement errors of 0.10 and 0.05 ergs; however, the amount of smoothing was significantly reduced. For example, in the 0.05 error case the departures above the frontal zone ranged from -30 to + 36 knots.

It is important to note that the results discussed above were obtained using a 1° latitude grid spacing. It is quite probable that measurements containing the assumed error mentioned above are not adequate for extracting meaningful thermal gradients from such a fine grid interval. In the next section the results obtained using various intervals of grid spacing are examined.

The Optimum Grid Spacing

To achieve the optimum results, a grid spacing which complements the observational capability of the instrument is required. Using the GGW-TUS cross section, accumulated temperature gradient departures for grid intervals of 1°, 2°, 3°, and 4° of latitude were calculated for assumed measurement errors of 0.25, 0.10 and 0.05 ergs and for climatological and 12-hour persistence first guesses. The procedures used were the same as those discussed previously except that the grid spacing varied.

The results, expressed as root-mean square (RMS) errors, for the various grid intervals, instrumental errors and initial guesses are shown in Figure 6. As expected, a grid spacing of 1° of latitude (111 km) produced the largest RMS errors for each of the three assumed measurement errors and for both initial guesses. A substantial reduction in the RMS error occurs when the grid spacing is increased to 2° of latitude (222 km). A further increase in grid spacing produces only a minor additional reduction in the RMS error. Figure 6 also demonstrates the superiority of the observations based on assumed measurement errors of 0.05 ergs. With respect to the two types of initial guesses used in the retrieval procedure, there is not a great deal of difference. Because there is no obvious gain in using a persistence guess rather than a climatological guess, the climatology initial guess is recommended. It is much easier to use operationally.

In attempting to resolve features as small as the jet streak, one is faced with a choice. When the grid interval is increased, the deleterious effect of measurement error is reduced; however, the resolution of the thermal support of the jet streak is also reduced. Consequently, a compromise involving the scale of the jet streak, the measurement error and the grid interval must be made. Happily, the choice is not a difficult

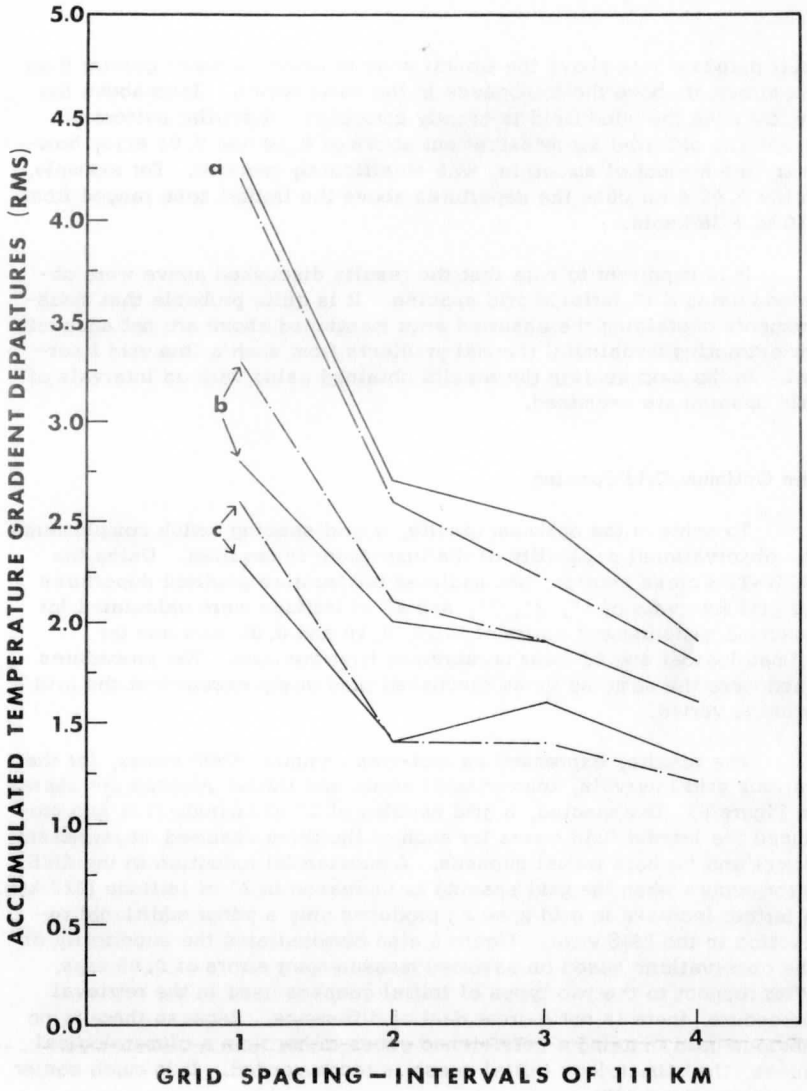

Figure 6. Root mean square values of accumulated temperature gradient departures as a function of grid spacing. Solid line is for climatological first guess and dashed line for 12-hour persistence first guess. Assumed satellite observational errors are: a) 0.25 ergs, b) 0.10 ergs, and c) 0.05 ergs.

one. The 2° latitude spacing and the 0.05 ergs instrument error are clearly superior.

Comparison of the Simulated and Retrieved Wind Fields

As noted previously, the spacing of conventional radiosonde stations, even in the United States, is often inadequate to locate a jet streak. Only through a careful, time-consuming isentropic cross sectional analysis can the feature be discovered. In Figure 7, isotachs representing the observed wind component normal to the GGW-TUS cross section are presented. The isotachs are based only on the wind observations from the five radiosonde stations. The northward and somewhat downward extension of the isotach maximum, located near 200 mb in the INW-TUS area, faintly hints that a second jet maximum may be present north of INW.

To better resolve the wind field, the GGW-TUS cross sectional isentropic analysis, the 700 mb geostrophic winds and the thermal wind relationship were used to construct the geostrophic wind field normal to the cross section. The results presented in Figure 8 show the wind field obtained when 1°, 2°, 3°, and 4° latitude grid spacings are used. A jet core is clearly portrayed in panels A and B (i.e., for 1° and 2° latitude spacings). While the core is still evident in panel C (3° latitude spacing), only one closed isotach could be analyzed. In panel D (4° latitude spacing) the core disappears; all that remains is a somewhat northward and downward extension of the isotach maxima found in the INW-TUS area. Thus panel D is not greatly different than the isotach analysis of the observed winds presented in Figure 7. This simply demonstrates that a 4° latitude spacing (444 km), which is about the distance between radiosonde stations, is inadequate to locate this jet streak. It is noteworthy that the 1° and 2° latitude spacings produced a geostrophic velocity core in excess of 140 knots, while the 4° latitude spacing and the analysis of the observed winds gave values of about 100 knots and 80 knots, respectively.

The winds obtained from the retrieval soundings using a climatological first guess and 2° latitude grid interval are presented in panels A, C, and D of Figure 9. The results shown in panel A are based on an assumed measurement error of 0.05 ergs, while those in panels C and D are for 0.10 and 0.25 ergs, respectively. Panel B, which is a reproduction of panel B of Figure 8, is included to provide a visual comparison between the geostrophic wind field obtained from the cross section and that retrieved using the SIRS algorithm. The results obtained using an assumed error of 0.05 ergs are better than those obtained from the 0.10 ergs error retrieval and much superior to those achieved using the 0.25 ergs error retrieval. An inspection of the data used in pre-

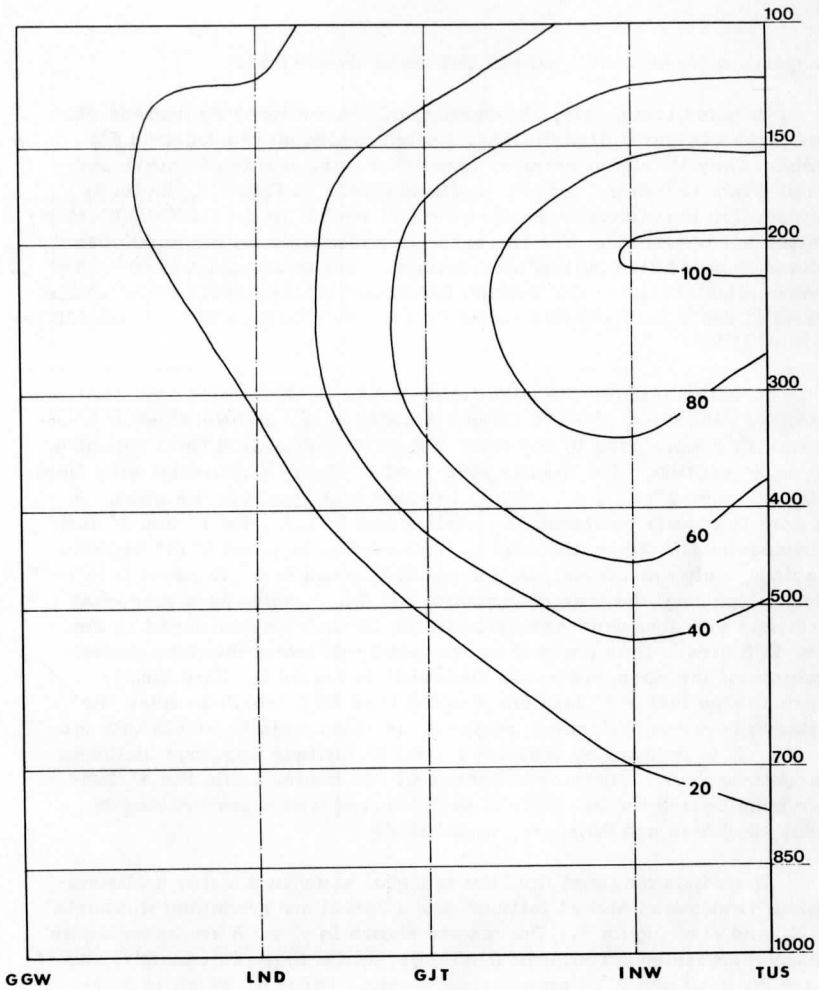

Figure 7. Isotach analysis of observed winds (from rawinsonde reports).

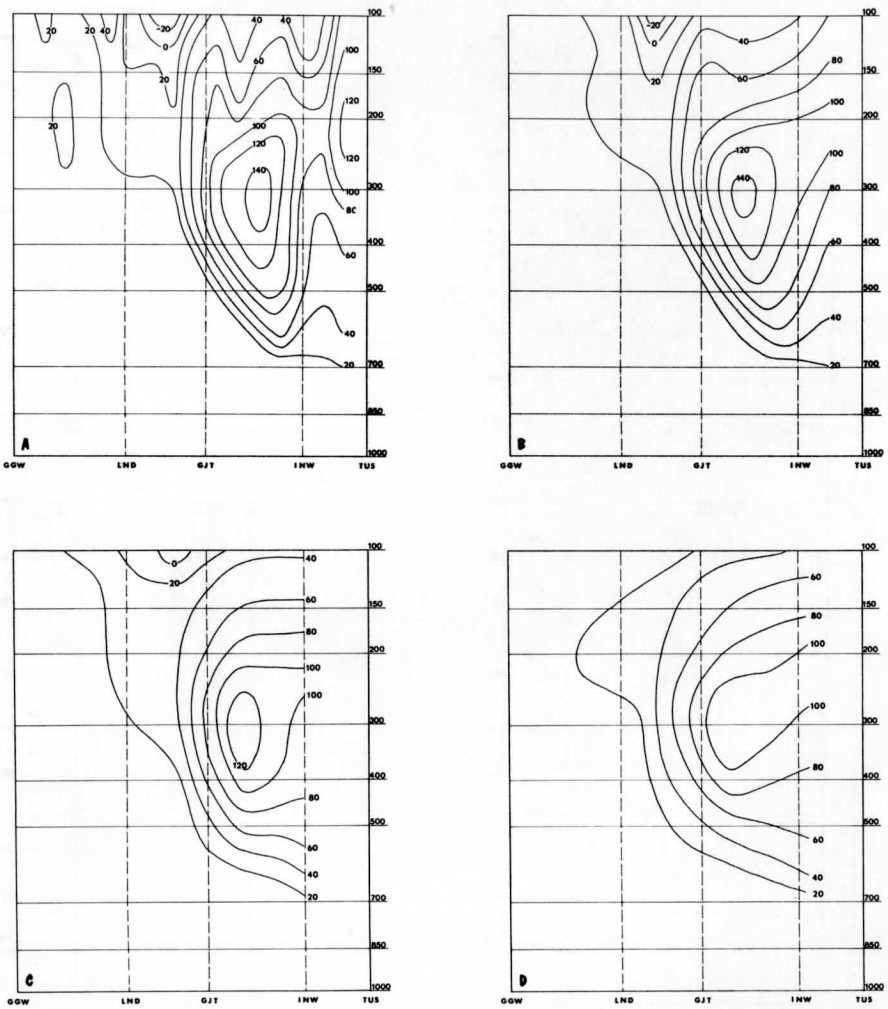

Figure 8. Isotachs of the geostrophic wind components (knots) obtained from the 12Z March 18, 1971 GGW-TUS isentropic cross-sectional analysis calculated for grid spacings of: A) 111 km, B) 222 km, C) 333 km, and D) 444 km. See text for further details.

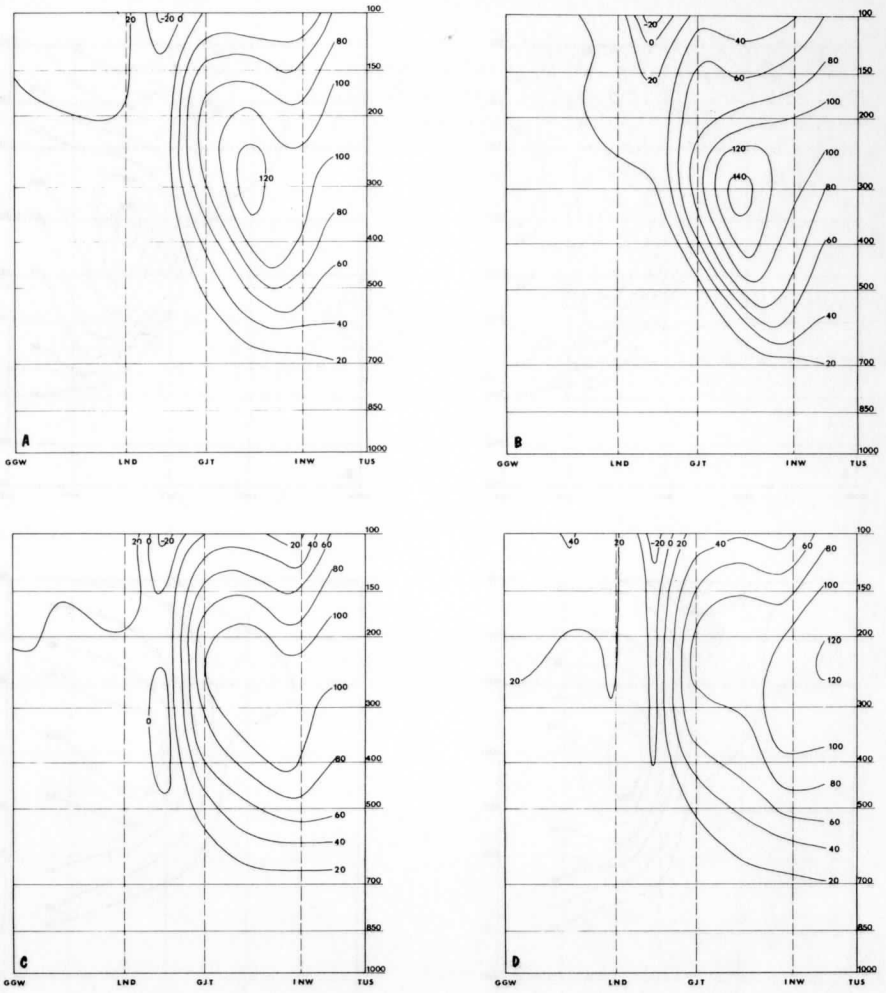

Figure 9. Isotachs of the geostrophic wind components (knots) along the GGW-TUS cross section obtained using the retrieved soundings. Results are based on a grid spacing of 222 km and assumed satellite observational errors of: A) 0.05 ergs, C) 0.10 ergs, and D) 0.25 ergs. Panel B, which is a reproduction of panel B of Figure 8, is included to facilitate comparison. See text for further details.

paring panels A and B revealed that the maximum velocity in the core was 142 knots for the computed geostrophic velocity and 126 knots for the retrieved value. Both occurred at the same sounding site and were within 25 mbs of each other. The actual wind at this point may have differed from these values which are based on the thermal wind relationship; however, it is not possible to obtain the actual wind at the point. It is not the purpose of this study to establish the reliability of the thermal wind. Rather, the objective is to determine the ability of the indirect sounding technique to resolve the thermal structure of the atmosphere in the jet streak region. The ability of the SIRS algorithm to achieve this excellent retrieval is indeed gratifying.

It is also worth noting that while the retrieval technique based on an assumed error of 0.25 ergs is unable to capture the jet core, it is able to retrieve a wind field comparable to the observed winds obtained from the rawinsondes or the geostrophic wind field computed from a 4° latitude grid spacing.

A Second Cross Section

The results of the previous section demonstrated the success of the SIRS algorithm in describing the atmosphere's thermal structure through the core of a jet streak. However, as discussed previously, there are pronounced longitudinal variations in the strength of the jet. To test the success of the retrieval method in obtaining the thermal structure in regions outside the core, a second isentropic cross section for 12Z 19 March 1971 was constructed.

The cross section, extending from Bismarck, North Dakota to Jackson, Mississippi is presented in Figure 10. As before, a detailed isentropic analysis was used to construct 18 synthetic soundings spaced at 1° latitude intervals along the cross section. Because of the optimum gradient information obtained from the GGW-TUS cross section, a 2° latitude grid interval was used in combination with a 0.05 ergs assumed measurement error to calculate the geostrophic winds and thermal gradients. Again, the 700 mb geostrophic winds were used in obtaining the geostrophic wind at higher levels. No attempt was made to resolve the wind field below 700 mb. An examination of the BIS-JAN cross section (Figure 10) shows rather diffuse baroclinity. Such a thermal structure is characteristic of the exit (or delta) region of a jet streak.

The isotachs of the observed winds normal to the cross section (shown in panel A of Figure 11) were based on wind reports from the six stations used in the cross section. A small low level maximum is noted near 800 mb above UMN (Monett, Missouri), and a broad, poorly defined maximum is found between Jackson (JAN) and Topeka (TOP) at 300 to 150

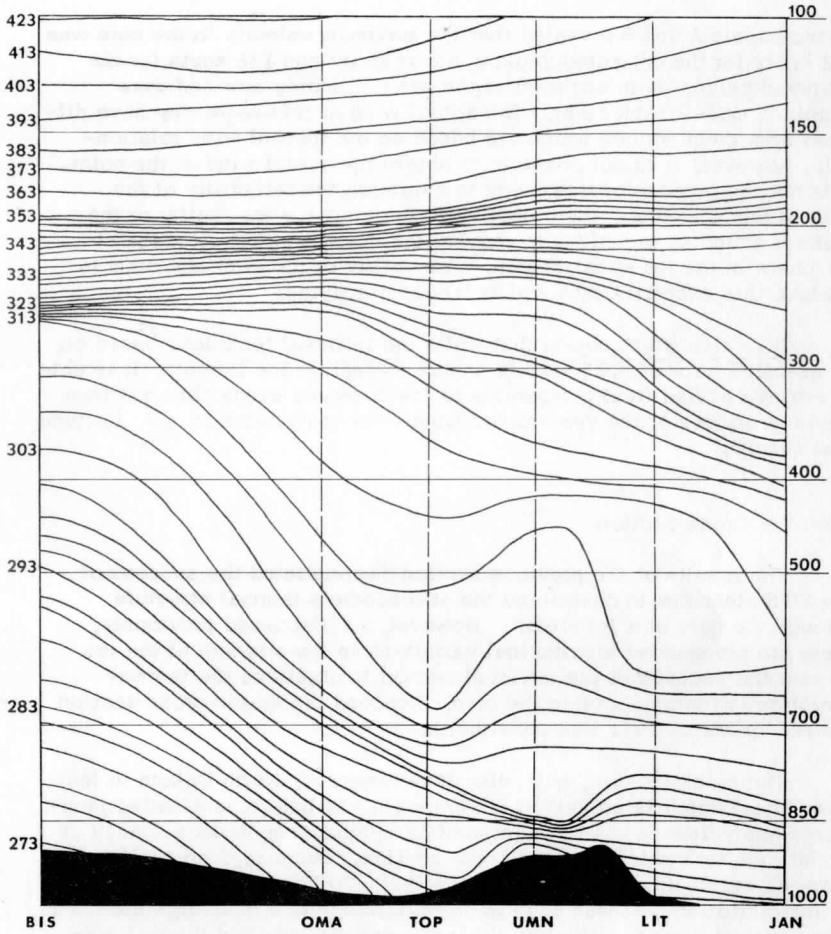

Figure 10. Isentropic cross section from Bismarck, North Dakota to Jackson, Mississippi for 12Z March 18, 1971. Isentropes at intervals of 2°C below 353°K and 10°C above 353°K.

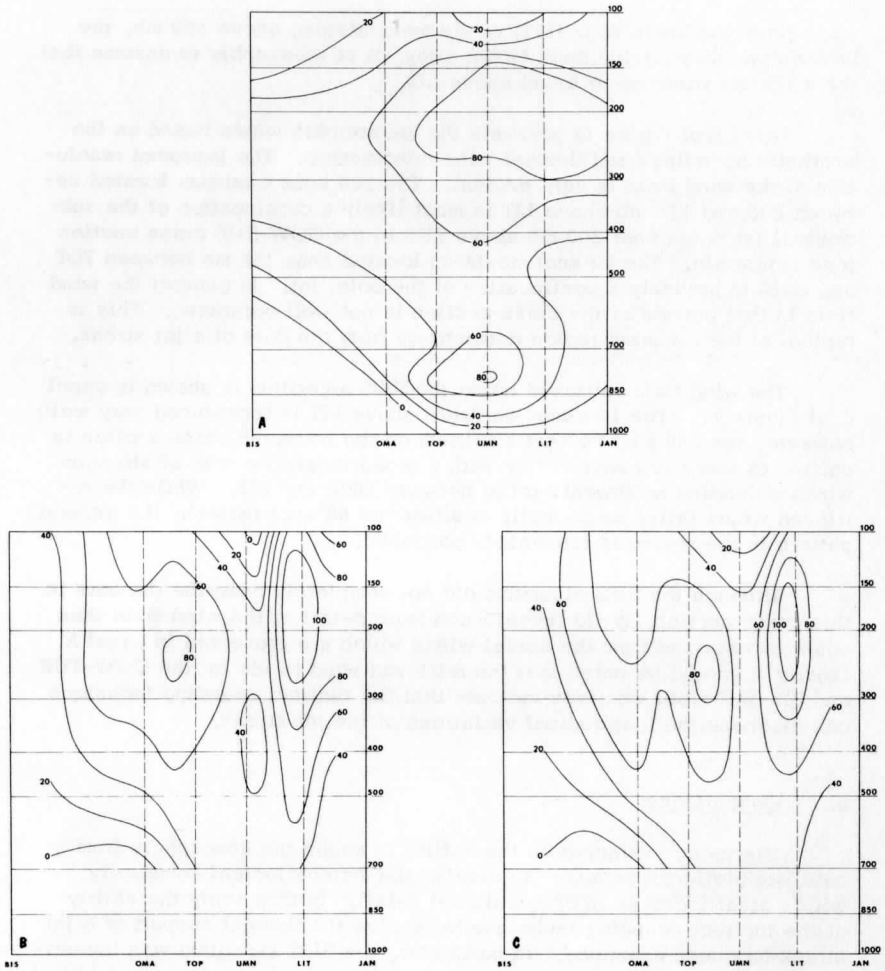

Figure 11. Isotachs of wind components normal to 12Z March 18, 1971 BIS-JAN cross section. A) Observed wind components (obtained from rawinsonde reports). B) Geostrophic wind components obtained from the cross section for a 222 km grid spacing. C) Geostrophic wind components obtained from the retrieved soundings for a 222 km grid spacing with an assumed observational error of 0.05 ergs and a climatological first guess.

mb. Since the Little Rock (LIT) winds were missing above 300 mb, the balloon probably having been blown away, it is reasonable to assume that the maximum winds were found above LIT.

Panel B of Figure 11 presents the geostrophic winds based on the synthetic soundings and thermal wind relationship. The improved resolution of the wind field is very evident. The 100 knot maximum located between 200 and 150 mb above LIT is most likely a continuation of the subtropical jet noted near 200 mb above TUS in the GGW-TUS cross section (see Figure 8A). The 80 knot maximum located near 250 mb between TOP and OMA is probably a continuation of the polar jet. In general the wind field in that portion of the cross section is not well organized. This is typical of the diffluent region downstream from the core of a jet streak.

The wind field retrieved using the SIRS algorithm is shown in panel C of Figure 11. The 100 knot maximum above LIT is reproduced very well; however, the 250 mb, 80 knot maximum on the retrieved cross section is shifted to just southeast of TOP with a broad indefinite area of stronger winds extending northwestward to between OMA and BIS. While the retrieved winds failed to correctly position the 80 knot isotach, the general pattern in the region is reasonably portrayed.

Although the SIRS algorithm did not completely describe the core in this cross section, it did reveal much more detail of the wind field than could be obtained from the actual winds which are presented in panel A. Finally it should be noted that the retrieved wind fields for the GGW-TUS and BIS-JAN cross sections indicate that the indirect sounding technique can diagnose the longitudinal variations of the jet streak.

6. Conclusions

The recent advances in the ability to sound the atmosphere from satellite platforms promise to provide the meteorological community with a great increase in observational detail. In this study the ability of the indirect sounding technique to resolve the thermal support of a jet streak has been examined. In particular, the SIRS algorithm was investigated assuming a variety of measurement errors, grid spacings and initial guesses. From the results of the case study the following conclusions and recommendations for future work are made:

1. The SIRS algorithm is quite successful in describing the general thermal structure of the atmosphere. With an assumed measurement error of 0.25 ergs it appears possible to retrieve the wind field with about as much detail as is provided by the current radiosonde network over the United States. Thus, it seems feasible that data-poor regions, such as the oceanic areas, may be successfully observed through indirect sensing techniques.

2. For an assumed error of 0.25 ergs the retrieval technique is incapable of resolving the thermal support of the propagating jet streak. However, measurements containing assumed errors of 0.10 and 0.05 ergs are capable of resolving the thermal support. The measurements containing an assumed error of 0.05 ergs, when used in conjunction with 2° latitude grid spacing, are especially impressive in their resolutive ability. A grid spacing of 1° of latitude introduces an excessive amount of noise, while 3° or 4° latitude spacings are insufficient to resolve the thermal support of the jet streak.

3. A weakness in the SIRS retrieval method is the inability to resolve temperature inversions. This weakness results in a smoothing of the strong vertical wind shears characteristic of jet streaks. The inclusion of a 4.3μm sensing channel in future instruments may aid in the resolution of temperature inversions. Additional study of the effect of including this channel is certainly warranted.

4. The success of the infrared sounding technique is dependent upon the retrieval of satellite observations in clear regions. In this study it was assumed that all the simulated satellite observations were from cloudless areas. Although the GGW-TUS cross section was for the most part free of clouds, the second cross section (BIS-JAN) was not. While the current SIRS instruments have a field of view of 225 km, the new upcoming instruments will have fields of view of 30-60 km. Although this will permit a larger number of cloud-free observations, it appears that the cloud problem will not be suitably solved until data from microwave channels are included.

5. In locating the jet streak, the use of indirect sounding retrievals from geosynchronous satellite observations may be especially valuable. Since the jet streak occupies a very limited area, it would be desirable to sense these critical areas in much more detail than the quiescent areas. A geosynchronous satellite is especially suitable for such variable sensing.

6. In this study moisture information was not included in the retrieval procedure. In future work the inclusion of such information may improve the accuracy of the retrievals.

7. While it was the purpose of this study to simply examine the ability of the indirect sounding technique to resolve the thermal support of the jet streak, the employment of the thermal wind relationship will be of great importance in retrieving the wind field from real data. Therefore studies which attempt to maximize the usefulness of the thermal wind relationship are certainly in order. Of equal importance is the need to obtain winds at some known level to serve as a base. For example, the Man-computer Interactive Data Access System (McIDAS) developed by Suomi et al. (1972) offers promise.

8. Finally, if these greatly improved wind measurements are to be optimally used in numerical models, revisions in the currently used objective analysis techniques may be required. Since the jet streak is a relatively long, narrow feature, an eccentric searching technique, such as that described by Deaven (1971), should seriously be considered for use in preparing the initial analysis for numerical models.

7. Acknowledgments

The authors gratefully acknowledge Dr. William L. Smith and Dr. Christopher Hayden for their helpful suggestions in approaching this study and their assistance in processing the data. They are also appreciative for the discussion of their work with Mr. David Barber and Dr. Donald R. Johnson. The assistance of Mr. Scott Singer in the data preparation and Miss Sandra Markevich in preparation of the final manuscript is also gratefully acknowledged. The research was supported by the National Environmental Satellite Service of the National Oceanic and Atmospheric Administration under grant number 1-35-229.

8. Bibliography

Cahir, J. J., 1971: Implications of circulations in the vicinity of jet streaks at subsynoptic scales. The Pennsylvania State University, Dept. of Meteorology, Ph. D. Thesis, 170 pp.

Deaven, D. G., 1971: An improved algorithm for objective analysis. The Pennsylvania State University, Dept. of Meteorology, M. S. Thesis, June 1971, 44 pp.

Duquet, R., E. F. Danielsen and N. R. Phares, 1964: Objective cross section analysis. Prepared for Air Force Research Laboratories, Office of Aerospace Research, Final Report (Part II), 20 pp.

Hanel, R. and B. Conrath, 1969: Interferometer experiment on Nimbus 3: preliminary results. Science, 165, 1258-1260.

Hanel, R., B. J. Conrath, V. G. Kunde, C. Prabhakara, I. Revah, V. V. Salomonson, and G. Wolford, 1971: The Nimbus 4 infrared spectroscopy experiment, IRIS-D part 1, calibrated thermal emission spectra. GSFC, NASA, preprint X-622-71-272 (submitted to J. Geophy. Res.).

Johnson, D. H. and S. M. Daniels, 1953: Rainfall in relation to the jet stream. Quart. J. R. Meteor. Soc., 80, 212-217.

Miller, R. C., 1967: Notes on Analysis and Severe-Storm Forecasting Procedures of the Military Weather Warning Center, Air Weather Service (MAC), U. S. Air Force, Technical Report 200.

Murray, R. and S. M. Daniels, 1953: Transverse flow at entrance and exit to jet streams, Quart. J. R. Meteor. Soc., 79, 236-241.

Newton, C. W., 1954: Frontogenesis and frontolysis as a three-dimensional process, J. Meteor., 11, 449-461.

Palmen, E. and C. W. Newton, 1969: Atmospheric Circulation Systems, Academic Press, 603 pp.

Riehl, J., J. Badner, J. E. Hovde, N. E. LaSeur, L. L. Means, W. C. Palmer, M. J. Schroeder, L. W. Snellman, and others, 1952: Forecasting in middle latitudes. Amer. Meteor. Soc. Monogr., 5, 80 pp.

Rieter, E., 1963: Jet Stream Meteorology, University of Chicago Press, 515 pp.

Smith, W. L., H. M. Woolf, and W. C. Jacob, 1970: A regression method for obtaining real-time temperature to geopotential height profiles, from satellite spectrometer measurements, MWR, 98, pp. 582-603.

Smith, W. L., H. M. Woolf and H. E. Fleming, 1972: Retrieval of atmospheric temperature profiles from satellite measurements for dynamical forecasting, J. Appl. Meteor., 11, 113-122.

Smith, W. L., 1972: Satellite techniques for observing the temperature structure of the atmosphere. Presented at: International Conference on Aerospace and Aeronautical Meteorology of the American Meteorological Society, May 22-26, Washington, D. C.

Starrett, L. G., 1949: The relation of precipitation patterns in North America to certain types of jet streams at the 300 mb level, J. Meteor., 6, 347-352.

Suomi, V. E. et al., 1972: An interim report on the development of the Man-computer Interactive Data Access System, Space Science and Engineering Center, University of Wisconsin, Madison, November 1972.

Wark, D. Q. and D. T. Hilleary, 1969: ESSA, atmospheric temperature: successful test of remote probing. Science, 165: 1256-1258.

_____, 1971: The satellite infrared and spectrometer (SIRS) experiment on the Nimbus III and Nimbus IV satellite. Presented at IAMAP/IUGG symposium on remote sensing, Moscow, USSR.

Yeh, T. -C., 1950: The circulation of the high troposphere over China in the winter of 1945-46. Tellus, 2, 175-183.